POWER ALLOCATION FOR SPATIAL OPTICAL-OFDM WITH DIMMING

POWER ALLOCATION FOR SPATIAL OPTICAL-OFDM WITH DIMMING

BY

DONGHAN LI, B.Sc.

A THESIS

SUBMITTED TO THE DEPARTMENT OF ELECTRICAL & COMPUTER ENGINEERING

AND THE SCHOOL OF GRADUATE STUDIES

OF MCMASTER UNIVERSITY

IN PARTIAL FULFILMENT OF THE REQUIREMENTS

FOR THE DEGREE OF

MASTER OF APPLIED SCIENCE

Master of Applied Science (2020) McMaster University

(Electrical & computer engineering) Hamilton, Ontario, Canada

TITLE:	Power allocation for spatial optical-OFDM with dimming
AUTHOR:	Donghan Li B.Sc., (Electronic Information Engineering), Jilin University, Changchun, China
SUPERVISOR:	Dr. Steve Hranilovic
NUMBER OF PAGES:	xiv, 102

To my family

Abstract

Light-emitting diode (LED) luminaires are ubiquitous and widely used in our daily life. Because of energy efficiency and illumination requirements, LED lamps are required to dim. In addition to the lighting function, visible light communication (VLC) is being considered as a potential technology beyond 5G. Orthogonal frequency-division multiplexing (OFDM) is a popular modulation choice and most recently spatial optical OFDM (SO-OFDM) has been used with multiple LEDs. SO-OFDM is a low complexity way of constructing OFDM signals by sending a series of narrow-band emissions from different LEDs and allowing them to sum in space. The integration of dimming within an SO-OFDM framework remains an open area of research.

In this thesis, an optimal dimming strategy for optical power allocation is proposed based on SO-OFDM in visible light communication systems under different illumination requirements, i.e., dimming. Firstly, a non-convex problem is formulated to maximize the capacity of SO-OFDM under a specified dimming target. Furthermore, this non-convex problem is broken into a group of convex problems through approximations and constraint relaxation.

The proposed scheme can optimize the power allocation in SO-OFDM and achieve the dimming target at the same time. According to the proposed power allocation

scheme, more of the power is allocated to subcarriers with low noise variance. This phenomenon makes sense to take advantage of good channels when power is limited and is similar to the conventional water-filling method. When the dimming target and signal-to-noise ratio (SNR) is sufficiently high, the optimal distribution approaches a uniform distribution which agrees well with conventional water filling in a high SNR regime. Compared with traditional digital dimming, the proposed spatial dimming method can not only use spatial domain for dimming but also allocates power to different subcarriers according to channel conditions which is more efficient. Analytical and numerical results imply that the proposed scheme converges quickly and performs well compared with traditional power allocation methods.

Acknowledgements

Two years passed, and my graduate life in the Department of Electrical and Computer Engineering at McMaster University was nearing completion. Recalling my two years of study and life, I not only learned knowledge and exercised my abilities, but also felt the teachers, family and friends support and care, I think, this should be the most precious asset I have learned from studying in Canada. Here, I would like to take this opportunity to express my gratitude to them.

First of all, I would like to thank my supervisor of Dr. Steve Hranilovic. He has a rigorous academic attitude and rich scientific research experience. At the same time, from the graduate course to the writing of the thesis, through his experience and knowledge, Dr. Steve Hranilovic taught us to broaden our horizons and strive to make progress, so that I have improved my ideological awareness.

At the same time, I would like to thank Mr. Bai Ruowen and Mohammed, who guided my graduation project, for answering all my questions patiently, constantly inspiring my research, and giving me a lot of directional guidance. So that I can successfully complete the thesis.

Next, thank friends and classmates around you. Thanks to Li Yawen, Zhang Yuxi Wang Tongjue, and other friends who helped me. Thank you for your selfless help in my study and life. With your help, I can overcome the difficulties in learning

again and again; I also want to thank my roommates for their care, tolerance, and understanding.

Finally, I would like to thank my parents who have developed good study habits for me since I was a child. You have been working tirelessly to support me and encourage me every time you encounter difficulties so that I have the motivation to move forward.

Thank you to everyone who has cared about and helped me!

Contents

List of Figures

List of Tables

Chapter 1

Introduction

Due to the increasing global electricity consumption for lighting [4], dimming technology is important in illumination for energy saving and to adjust to user requirements. Visible light communication (VLC) technology is an emerging technology to allow for a secondary use for light-emitting diode (LED) luminaires that use modulated light from luminaires to transmit information while providing illumination. Integrating VLC with the necessary dimming functionality from illumination is an ongoing issue. Among the many modulation technologies, optical orthogonal frequency-division multiplexing (OFDM) technology has recently been considered coupled with VLC given that it provides both high-speed and highly reliable VLC channels. However, OFDM also suffers from the high peak-to-average power ratio (PAPR) [4]. More recently, spatial optical-OFDM (SO-OFDM) has been proposed to reduce the PAPR by separating the OFDM symbols over multiple LEDs in the luminaires thereby reducing PAPR[8]. In particular, this thesis develops optimized dimming strategies based on SO-OFDM to jointly satisfy illumination constraints and maximize the capacity considering a band-limited channel.

1.1 Overview of visible light communications

This section describes the overview of lighting systems for VLC technology and introduces the development status of VLC. Additionally, the problem VLC is facing when integrated with other technologies is also discussed.

1.1.1 Introduction of visible light communication

In recent years, due to the explosive growth of technologies such as cloud computing, artificial intelligence (AI), virtual reality (VR) and the Internet-of-Things (IoT), the demand for wireless data traffic has also continued to increase accordingly [9]. In [10], Cisco's Visual Network Index (VNI) predicts that global mobile data traffic is growing rapidly at a compound annual growth rate (CAGR) of 46%. By 2022, global mobile data traffic will reach 77.5 exabytes per month and data traffic from wireless and mobile devices will reach 71% of global total IP traffic [10]. As an emerging technology with broad-spectrum resources of nearly 400THz, VLC has received widespread attention in the 5th generation wireless systems (5G) [11].

Visible light communication is a relatively new optical wireless communications (OWC) technology that uses visible light as an information carrier without optical fibre or other wired transmission media to directly transmit optical signals in free space. VLC technology can also take full advantage of the existing LED illumination facilities which makes VLC more pervasive [12]. The electromagnetic spectrum distribution is shown in Figure 1.1 [1] which illustrates that VLC systems have a wide available frequency band. These features make VLC systems attractive to provide a primary illumination role together with a secondary communication role via VLC.

Figure 1.2 illustrates a block diagram of the VLC system which can be divided

Figure 1.1: Schematic diagram of electromagnetic spectrum distribution [1]

into three parts: Transmitter, free-space channel and receiver [13].

At the transmitter, signals are transmitted by modulating the optical power of LEDs by using intensity modulation (IM) as shown in Figure 1.2. Firstly, transmitted signals are encoded and then digital signals are converted into analog signals through a digital-to-analog converter (DAC). Additionally, filtered signals are subjected to a suitable direct current (DC) signal drives LED for electro-optical conversion. The optical intensity signal reaches the receiver of the system after being transmitted in free space [14].

At the receiver, the collected signal reaches the photodiodes (PDs) which convert the received optical power into corresponding current [15] and perform the photo-electric conversion. After filtering the electrical signal, an analog-to-digital converter (ADC) converts the analog electrical signals into digital signals and corresponding signals are recovered at the receiver [16]. Intensity modulation and direct detection (IM/DD) is used as the main modulation and demodulation method in VLC systems [14]. It is a direct envelope detection of the intensity-modulated wireless signal. That is to say, the intensity-modulated signal can be conveyed through the intensity of LEDs and detected by photodiodes (PDs) directly at the receiver [17]. For IM/DD systems, a modulated signal is directly added on the DC bias current [18] directly modulating the intensity of light [19]. The intensity of LEDs is proportional to the

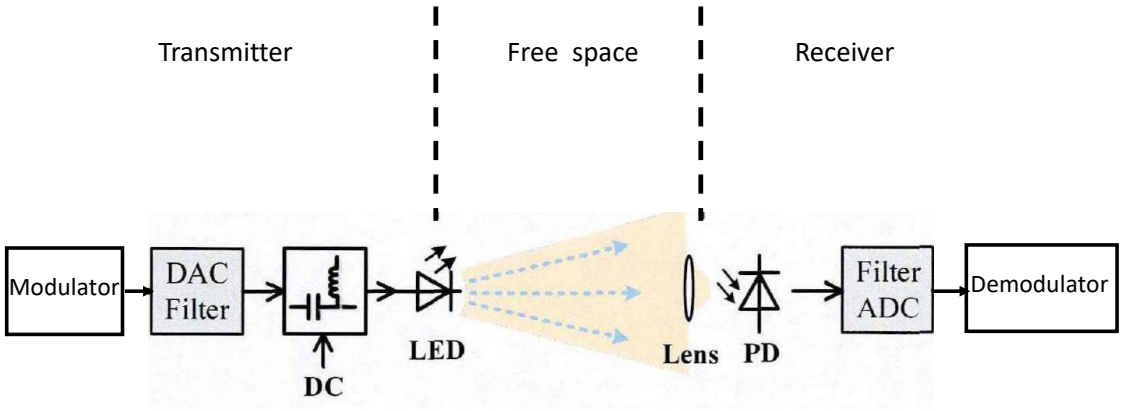

Figure 1.2: Block diagram of VLC system

current through the LEDs. The power constraint is equal to the average amplitude of the emitted waveform. Therefore, transmitted signals in VLC using IM/DD should have positive amplitude, be real valued and constrained in their mean value.

1.1.2 History of VLC

The earliest VLC activities can be traced back to 1880 when Alexander G. Bell developed the "Photo-phone", which can transmit voice information by using the reflection of sunlight from a metal plate [20]. In the 1970s, F. R. Gfeller published a paper about wireless infrared networks where a new wireless channel is proposed to achieve data transmission of different in-house terminals [5]. Beginning in 2000, the research group of Dr.Nakagawa at Keio University in Japan proposed the use of white LED lights to implement indoor access networks [21] and established a theoretical model of indoor visible light communication system [22]. Since 2008, the United States launched the 'Smart Lighting Project' and has researched key issues in VLC with more than 30 top US universities including Boston University and the Georgia

Institute of Technology [23] [24] [25].

1.1.3 Standards for VLC

In 1993, the Infrared Data Association (IrDA) was established to launch standards for short-range wireless communications [26]. In the standardization of VLC, Japan established the Visible Light Communications Consortium (VLCC) in 2003 and launched the Japan Electronics and Information Technology Industries Association (JEITA) 1221 standard in 2007, which specifies the scope and use of three visible light frequency bands [27]. The standards committee released the first VLC Personal Area Networks (VPAN) standard [28] which supports high-data-rate up to 96 Mb/s in VLC systems [29]. The standard also takes into account human safety which provides flicker-free VLC [29] where flicker is discussed more depth in Section 1.1.6. To meet the specific needs of VLC in practical home applications, the European Union and more than twenty scientific research institutions released the OMEGA [30] standard with Port Physical Layer (PHY) architecture. The standard takes into account the quality of service, communication mobility and practical problems in high-speed transmission processes such as compatibility with traditional communication technologies [30]. Due to the gradual development of VLC technology, the IEEE 802.15.7R1 working group was established in 2015 [31] which determines the high-speed VLC application scenario standard [32]. In 2017, IEEE 802.15.13 working group was established to realize the requirements of wireless private networks with a transmission distance of about two hundred meters under a data rate of 10Gb/period [33]. In 2018, the IEEE 802.11bb Task Group (TG) was established which focuses on light-based communications[34]. The IEEE 802.11bb TG specifies a new physical

layer and at least one operation mode of the new physical layer can achieve a single link throughput of at least 5 Gb/s [35].

Commonly used VLC modulation techniques include On-Off Keying (OOK) [36], variable pulse position modulation (VPPM) [24], Color Shift Keying (CSK) [37], Carrier less Amplitude Phase Modulation (CAP) [4] and Orthogonal Frequency Division Multiplexing (OFDM) [38]. OOK is widely used in early visible light communication systems because it is easy to implement where 'ON' and 'OFF' pulses can present the binary bits [37] [4]. There are two widely used modulation methods in PM: pulse position modulation (PPM) and pulse width modulation (PWM) [39]. For pulse position modulation, the position of each pulse is controlled by a modulation signal, so that the relative position of each pulse conveys information. The amplitude and width of the pulse in the pulse sequence remain unchanged. PWM is pulse width modulation. The width of each pulse in the pulse sequence is controlled by a modulation signal and the duration of each pulse is proportional to the modulation signal. The IEEE 802.15.7 standard recommends the use of VPPM modulation format to achieve dimming VLC which uses the combination of 2-PPM and PWM. VPPM can be widely used in VLC systems since it can control the brightness of LEDs easier than PPM [40]. By adjusting the pulse width, any brightness target (i.e., average amplitude) can be achieved. By changing the position of each pulse without changing its amplitude, the function of data transmission can be realized. The above modulation techniques are susceptible to inter symbol interference (ISI) [24], which promotes the research of OFDM technology in VLC systems as the core technology of the fifth generation of mobile communication technology standards (5G) and sixth generation of mobile communication technology standards (6G).

1.1.4 Comparison of VLC and radio frequency (RF) channels

Facing the increasing traffic demand, traditional radio frequency (RF)-only wireless communication has an increasingly serious issue with spectrum scarcity [4]. Since VLC does not interfere with the RF frequency band, it is expected to effectively complement RF wireless communication [12] [41].

Compared with traditional RF communication technologies, visible light communication can make full use of existing lighting facilities for communication [6] and illumination due to its broad spectrum and other characteristics as shown in Table 1.1. However, RF communication is still the primary wireless communication method [42]. As shown in Table 1.1, RF communication is a mature technology compared with VLC while VLC systems can achieve illumination and communication at the same time [25]. Electromagnetic interference (EMI) is a serious issue especially in RF internet-of-things deployments with a high density of transceivers. VLC transmissions have immunity to EMI for sensitive electronic systems since it operates at optical frequencies while RF communication will be disturbed [43]. For example, VLC systems can be widely used in hospitals where EMI must be avoided [15]. However, VLC systems must still compensate for optical interference [44]. For instance, if two VLC devices are in the same room, the two devices will interfere with each other [45].

The wavelength of visible light is about 400nm to 700nm, and the corresponding available spectrum is about 430THz to 790THz [6]. The available spectrum of RF is 3kHz-300GHz, and the shortest wavelength of radio frequency is about 1mm [6]. Since the wavelength of visible light is shorter than that of RF electromagnetic waves, its diffraction is smaller and a more directive antennae can be constructed. However, optical emissions are typically contained by opaque boundaries of rooms

Table 1.1: Comparison of traditional RF communication and Visible Light Communication [6]

Criterion	VLC	RF Communication
Services	Illumination and Communication	Communication
Coverage	limited	Mostly wide
Standards	mainly IEEE 802.15.7, IEEE 802.15.13 and IEEE 802.11bb	Matured
Distance	Short	Long
EM Interference	No	Yes
Spectrum	430THz to 790THz	3000Hz to 300GHz
Security	Good	Poor

which can fill some applications indoors such as high-speed downlink and operation in dense interference-limited environments [25]. For instance, VLC emissions cannot penetrate opaque surfaces, such as walls [25]. Therefore, visible light communication is often used for short-distance communication, such as indoor communication. RF communication is more appropriate for long-distance mobile communications.

1.1.5 Industrial uses of VLC

Driven by broad market prospects, companies such as PureLiFi [1] , Philips [46] and Velmenni [47] are working on the development of VLC systems. In 2011, Professor H. Haas and his team established the company PureLiFi, dedicated to the production of Li-Fi products and the promotion of Li-Fi technology [1]. The products LiFi-XC can achieve the speeds of several Gbps in communication devices [1]. What is more, VLC has a very wide range of applications in all walks of life. Philips proposed a VLC indoor positioning system based on LED indoor light source [47]. Signify (the newly renamed Philips Lighting Research branch) also has VLC products like Trulifi [46]. Velmenni's LiFi based optical wireless backhaul technology for FTTx can deliver the

throughput of about 1 Gbps [48]. Intelligent transportation systems (ITS) reduce traffic accidents, traffic jams and fuel consumption by obtaining and transmitting information about traffic conditions in time.

1.1.6 Integration of VLC with Lighting

In lighting systems, the ability and quality of illumination for the lighting system can be represented by some key properties such as colour rendering index (CRI), illumination level (dimming level) and colour temperature (CT) [49].

Colour rendering properties can be defined by the effect that a light source has on the hue of the perceived colour of the object [50]. For example, when an individual observes an object, the perceived hues depend on the illumination source of it [50].

Dimming means adjusting the brightness of luminaires according to the requirement for brightness levels in the workplace [50]. Under the constraint of illumination level, dimming control has been explored vastly as a vital illumination task [51]. The illumination requirements of the indoor environment are related to the different application scenarios. In general, the dimming level required for daily reading in classrooms is about 300 lux and for using computers, the dimming level required is merely 30 lux [52].

Flicker is a health hazard for users which is defined as the visible change in time of the brightness of an illumination device [53]. A large number of studies have found that light source flickering is closely related to neurological diseases. For example, migraine and flicker can induce seizures in some individuals [49]. For most people, the light flicker below 80 Hz can be perceived distinctly and human eyes can feel the change in brightness of light source at this time, which is unacceptable for illumination

[54].

Traditional luminaires include fluorescent lamps and incandescent lamps. Compared with typical luminaires, light emitting diodes (LEDs) are used in luminaires since LEDs have many advantages. For example, LEDs have a large light output for a given input electrical power which is more energy-efficient [55] compared with typical luminaires. LEDs also have longer service life, better durability and smaller size [56] [22].

The communication function of VLC is possible by modelling the intensity of the LEDs. VLC is a secondary application of luminaires and the communication function should be considered in the context of illumination constraints [56]. To integrate illumination and VLC, the LED equipment is used in VLC systems. Switching 'on' and 'off' for LEDs can be used to transmit information by modulating '0' and '1' to different states of LEDs [57].

LEDs can switch at high speed to ensure that the human eye will not perceive flicker which maintains the illumination function of VLC systems [58]. In practice, dimming of illumination can be realized by changing the average current of LEDs in VLC systems according to requirements for brightness levels in the workplace and daily life [59]. Therefore, a visible light communication system based on LEDs can provide a communication function while meeting illumination conditions simultaneously.

As discussed in Section 1.1.5, many industrial products use LEDs in VLC systems to achieve communication and illumination such as Trulifi and PureLiFi [46].

1.2 Optical OFDM Modulation Technology

1.2.1 Introduction of optical OFDM

OFDM is a type of multi-carrier modulation (MCM) that achieves modulation and demodulation based on inverse fast Fourier transform (IFFT) and fast Fourier transform (FFT) respectively [60]. The main idea of OFDM is to divide the channel into orthogonal sub-channels and convert high-speed serial data signals into parallel low-speed sub-signals [61]. Additionally, the parallel signals are used to modulate multiple orthogonal subcarriers respectively, to transmit signals in these sub-channels synchronously. Since the bandwidth of each sub-channel is only a small part of the original channel bandwidth, channel equalization is simplified [62]. Due to the orthogonality of the subcarriers, the frequency interval is very small which makes the frequency band utilization rate high [62]. A cyclic prefix (CP) is a cyclic structure added to the start of every OFDM frame which repeats the last k samples from the output where k is the memory of the channel. Formed by copying a piece of data after a data symbol to the front of the symbol [63] [64]. The CP allows for a simpler equalization by a single complex multiplication in the frequency domain at the receiver. It allows linear convolution of the channel to be equivalent to circular convolution making equalization in frequency domain a single complex multiplication.

In order to transform the original bipolar OFDM signal into a positive real OFDM signal, which is necessary for IM/DD channels, a wide variety of optical OFDM techniques have been proposed. The difference in the performance of existing optical OFDM techniques mainly stems from the different methods of achieving positive and real signals.

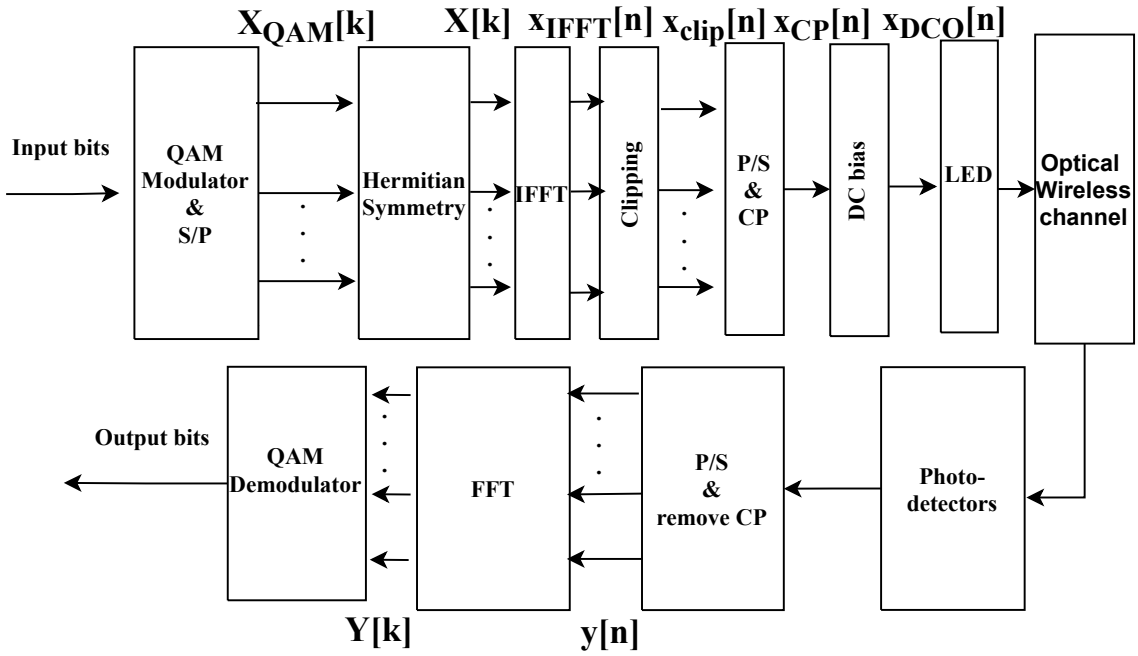

Figure 1.3: Block diagram of DCO-OFDM system [2]

.

Introduction of DCO-OFDM

Direct current biased optical OFDM (DCO-OFDM) is the most basic form of optical OFDM technology as shown in Figure 1.3. At the transmitter, the transmitted bit stream is mapped according to quadrature amplitude modulation (QAM) to yield the complex QAM symbols $X_{\mathrm{QAM}}[k]$, where $k \in \{1, 2, ..., N-1\}$. To ensure that the generated OFDM signals are real, the signals in the frequency domain (i..e, prior to IFFT) should have Hermitian symmetry which can be denoted as

$$X(k) = X^*(N-k), \quad 0 < k < N/2, \tag{1.2.1}$$

where N means the total number of subcarriers and k indicates the k-th subcarrier. The time-domain DCO-OFDM signal $x_{\mathrm{IFFT}}[n]$ after IFFT can be obtained as:

$$x_{\mathrm{IFFT}}[n] = \frac{1}{\sqrt{N}} \sum_{k=0}^{N-1} X[k] \exp\left(\frac{j2\pi kn}{N}\right), \tag{1.2.2}$$

where $x_{\mathrm{IFFT}}[n]$ means the n-th time-domain signal.

Subsequently, the output signals are hard clipped to fit the dynamic range of the LED which causes clipping distortion [65]. The dynamic range is the nonlinear LED transfer characteristic as shown in Figure 1.4 [3]. In Figure 1.4 x-axis represents the drive current input to the LEDs and the y-axis represents the output of corresponding optical power. As shown in Figure 1.4, the dynamic range of each LED is $[I_{\mathrm{L}}, I_{\mathrm{U}}]$ where I_{L} and I_{U} means the minimum and maximum drive current of the achievable linear range for a LED. The red dashed line represents the nonlinear LED response, as a comparison, the blue solid line represents the linearized response [3]. When the input amplitude of LEDs is in the non-linear region of the LED, such as $I_{\mathrm{nonlinear}}$, the relationship between the input amplitude and the output optical power is non-linear. Non-linear distortion will degrade the bit error rate (BER) performance of the Optical OFDM (O-OFDM) signal. Therefore, signals outside the dynamic range of the LED should be clipped to prevent the distortion of OFDM signals.

The clipped signal x_{clip} can be defined as

$$x_{\mathrm{clip}}[n] = \begin{cases} I_L, & x^{(\mathrm{D})}[n] < I_L \\ x_{\mathrm{IFFT}}[n], & I_L \leqslant x_{\mathrm{IFFT}}[n] \leqslant I_{\mathrm{H}} \\ I_{\mathrm{H}}, & x_{\mathrm{IFFT}}[n] > I_{\mathrm{H}} \end{cases} \tag{1.2.3}$$

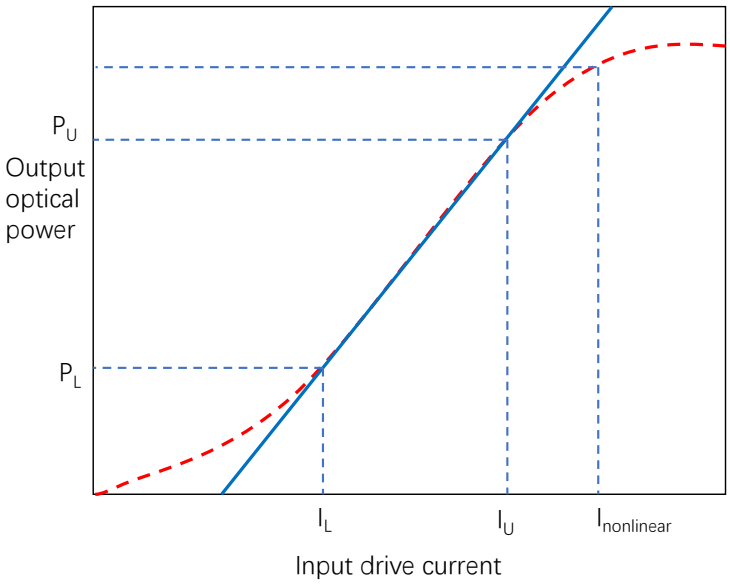

Figure 1.4: Nonlinear LED transfer characteristic [3]

After obtaining bipolar real signals, x_{CP} can be obtained by adding a cyclic prefix as discussed in Section 1.2. In order to obtain uni-polar positive signals, a DC bias I_{DC} is added to obtain the uni-polar positive signal x_{DCO}:

$$x_{\mathrm{DCO}}(n) = \begin{cases} x(n)_{\mathrm{CP}} + I_{\mathrm{DC}}, & x(n)_{\mathrm{CP}} \geq -I_{\mathrm{DC}} \\ 0, & x(n)_{\mathrm{CP}} < -I_{\mathrm{DC}}. \end{cases} \tag{1.2.4}$$

I_{DC} can be set as

$$I_{\mathrm{DC}} = \mu\sigma \tag{1.2.5}$$

where μ is a positive real number and σ is the standard deviation of $x[n]$ [26].

Finally, the clipped and biased signals from each group will drive the LEDs of each group accordingly. DCO-OFDM signals are then used to drive the LED to achieve Electro-Optical conversion (E/O). After the signal is transmitted through the optical channel, a photo-detector (PD) at the receiving end converts the received optical signal into an electrical signal and then conducts the corresponding signal demodulation for the electrical signal.

Introduction of ACO-OFDM

For asymmetrically clipped OFDM technology (ACO-OFDM), the modulation and demodulation process is similar to that of DCO-OFDM. ACO-OFDM only transmits data on odd subcarriers and sets zeros on even subcarriers [66]. By modulating odd subcarriers and setting even subcarriers to 0, a real, anti-symmetric time-domain signal is obtained after IFFT with the cost of one-half of spectrum efficiency loss [67]. The negative components of the time-domain OFDM signal can be clipped to obtain positive and real signals. However, clipping of the negative signal will not lose the

useful data and clipping noise can be shown to reside only on the even subcarriers [68].

In [69], asymmetrical hybrid optical OFDM is proposed which combines ACO-OFDM and pulse-amplitude-modulated discrete multitone (PAM-DMT), making full use of the limited dynamic range of LEDs over a wide dimming range. In [13], layered ACO-OFDM (LACO-OFDM) hybrid dimming scheme is discussed where an optimization problem of DC-bias to maximize the channel capacity is established. LACO-OFDM divides subcarriers into layers and compared with ACO-OFDM, the spectrum efficiency can be nearly doubled. Since there is no need to add DC bias, the power efficiency of LACO is higher than DCO-OFDM [70]. In addition, there are many other optical OFDM modulation methods proposed for high spectrum efficiency, including multi-layer IFFT enhanced U-OFDM (eU-OFDM) [71], asymmetrically clipped absolute value optical OFDM and polar OFDM (P-OFDM) [72] [73].

Although optical OFDM technology has many advantages, it also has some problems during transmission. The peak-to-average power ratio (PAPR) is defined as the ratio of signal peak power to its discrete signal average power. For the OFDM signal, because the signal amplitude is Gaussian distributed and the signal peak power is larger than the average power, which results in the large peak-to-average ratio (PAPR) [2]. Since the dynamic range of general power amplifiers is limited, OFDM signals with a relatively large PAPR can easily enter the nonlinear region of the power amplifier, which will result in nonlinear distortion [74].

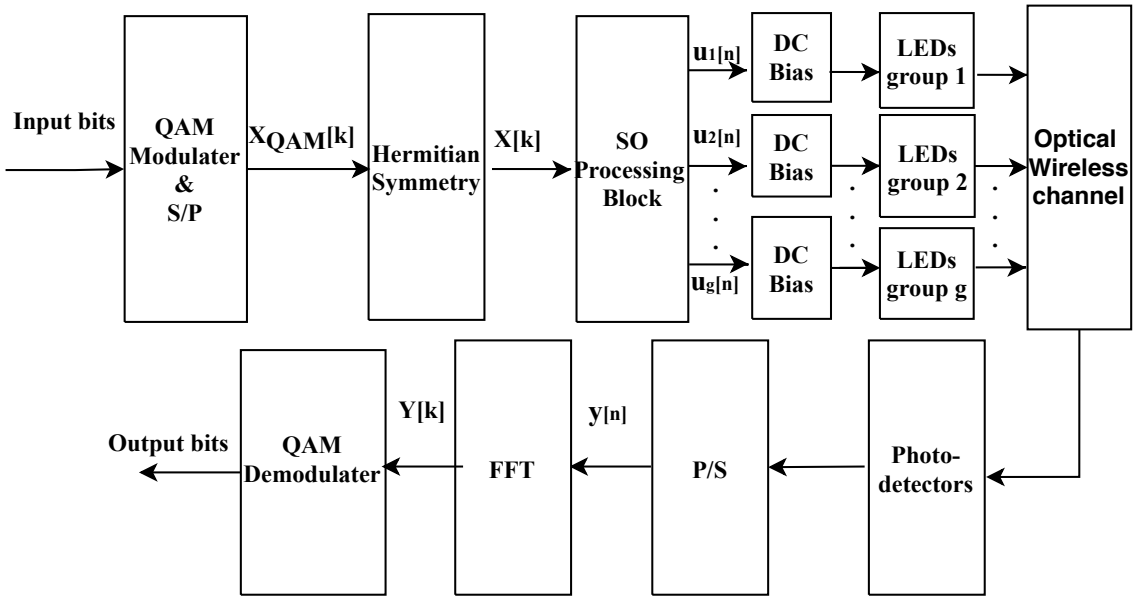

Figure 1.5: Block diagram of SO-OFDM system with L_g LEDs in G groups [2]

.

1.2.2 Spatial summing optical-OFDM

Spatial summing optical-OFDM (SO-OFDM) is an approach for PAPR reduction which leverages the unique spatial summing method. The key concept behind spatial summing optical-OFDM is to separate a wide-band input signal amongst different groups of LEDs [2]. In this way, high PAPR OFDM signals will be partitioned into many low-PAPR narrow-band signals are transmitted from multiple LEDs. Signals can be summed in the free-space before received [4].

The architecture of SO-OFDM is illustrated in Figure 1.5 [2]. There are L LEDs in total and the LEDs are separated into G groups. At the transmitter, the transmitted bit stream is mapped according to quadrature amplitude modulation (QAM) and get the complex QAM symbols $X_{\mathrm{QAM}}[k]$ firstly, where $k \in \{1, 2, ..., N-1\}$. Complex-value QAM symbols from the serial-to-parallel conversion are input the Hermitian

Symmetry block to get real-time domain OFDM signal. The spatial processing block divides the input wideband OFDM frame $X[k]$ into groups of narrow-band signals. Bipolar real time-domain spatial dimming OFDM signals will be obtained by using inverse fast Fourier transform (IFFT) and the parallel-to-serial conversion (P/S). Subsequently, the output signals will be hard clipped to ensure that their current range is between the dynamic range of LEDs.

Similar to the approach discussed in Section 1.3, the DC-bias should be added I_{DC} after clipping the symbols to make sure that the time domain signals are non-negative. I_{DC} can be set as

$$I_{\mathrm{DC}} = \mu\sigma_g, \tag{1.2.6}$$

where μ is a positive real number and σ_g^2 is the variance of g-th group [26]. A fixed bias is added for each symbol which is simpler to implement resulting in a non-zero probability of clipping. Finally, biased signals are clipped from each group and signals will drive the LEDs of each group accordingly.

Outputs from groups of LEDs sum in free-space and propagate to a standard OFDM receiver with a single photodiode (PD) as shown in Figure 1.5 [8]. The received signal from the PD is delivered to a parallel-to-serial (P/S) block. In the subsequent stage, a fast fourier transform (FFT) block will transform the time domain signals $y[k]$ into frequency domain signals $Y[k]$. Finally, the QAM demodulator block decodes the transmitted data.

1.3 Dimming techniques

This section presents a review of dimming approaches for LED luminaires dimming technologies of LEDs and introduces the influence of VLC systems when integrated with dimming control. Dimming techniques are effective ways to conserve energy for the illumination device and achieve the brightness requirements of people in different scenarios [36]. By using dimming schemes, the brightness of LED lamps can be adjusted to implement the dimming level, which makes lamps generate less heat and have a longer lifetime [36]. Since LEDs are current-driven devices, their brightness is proportional to the forward current through LEDs. In order to adjust the brightness of LEDs, the average power of LEDs can be changed by adjusting the drive current according to a dimming target [4]. However, because dimming will adversely affect communications, the main function of the VLC system cannot be neglected which makes sure the illumination and the data communication of the system [75].

Traditional dimming approaches can be mainly divided into analogue dimming (AD) and digital dimming (DD) [4]. In recent years, spatial dimming (SD) technology has also been studied, which can use the spatial domain of the LED to achieve optical power adjustment and dimming target [76] [77].

1.3.1 Analogue dimming

The essence of analogue dimming is to change the amplitude of the LED drive signal which can achieve the amplitude constraints of the system. As shown in Figure 1.6, the x-axis represents time, the y-axis represents driving current, the dashed line represents I_{bias}, and the solid line represents the implementation principle of different dimming methods. For analogue dimming in Figure 1.6, also known as amplitude

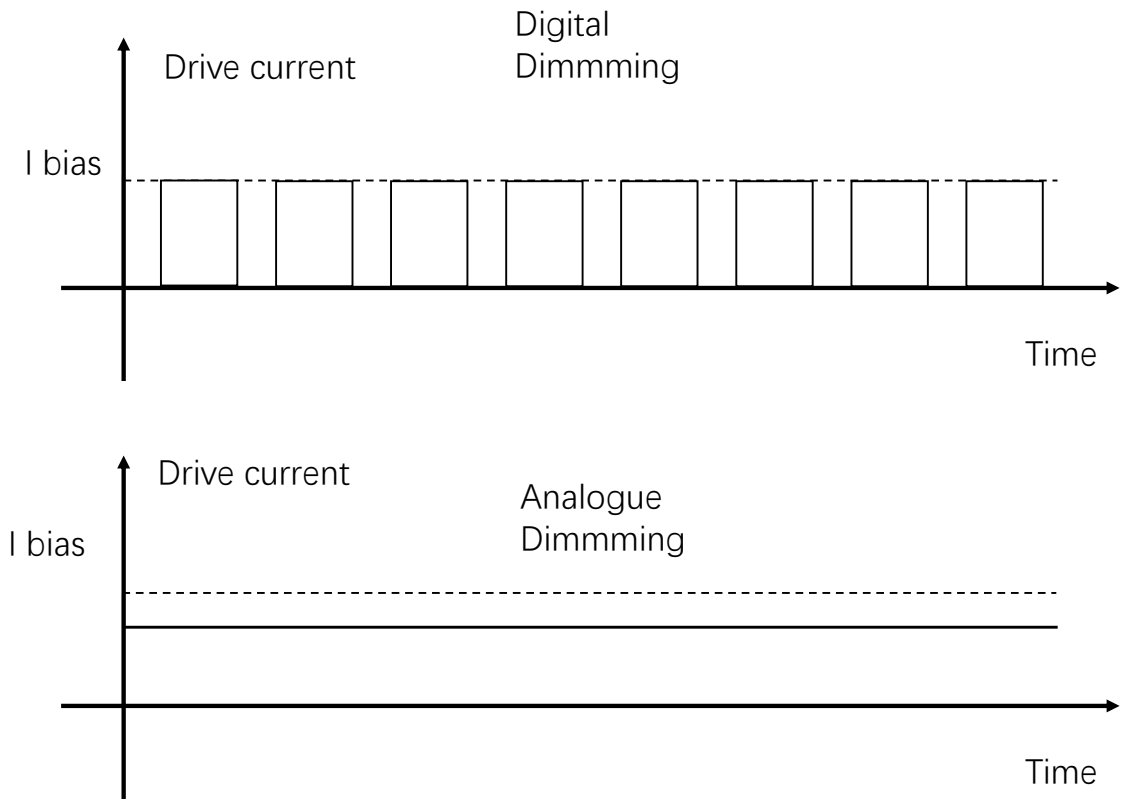

Figure 1.6: Principle of visible light analogue dimming and digital dimming technology [4]

modulation (AM), adjust the light intensity of LEDs luminaires to attain the dimming target by varying the DC source of LEDs [78]. In this way, the intensity of the light emitted by LEDs will change with the magnitude of the current to achieve dimming [79]. So the advantage of analog modulation is that the receiving device is simple and relatively easy to implement [4].

However, when the dimming target is near the upper or lower dynamic range limits, the communication performance will be confined considering the dynamic range of LEDs [51]. Accordingly, this may also result in chromaticity shift varying with the change of the forward current [4]. So using this method to adjust the brightness of the LED has an additional challenge of potentially changing the spectral and color temperature for LEDs [80] [81].

1.3.2 Digital dimming

Digital dimming is the approach used most frequently in the commercial dimming of luminaires. The essence of digital dimming is to adjust the DC content of the drive signal by changing the duty cycle of signals to achieve the required level. Although electromagnetic interference is possible due to the rapid changes in current [82], digital dimming can be viewed as a simple digital-to-analogue conversion technique. Digital dimming is also known as pulse width modulation (PWM) dimming which turns LEDs on and off to modify the on-time of the forward current and achieve brightness adjustment [83]. Taking into account these two characteristics, PWM achieves the dimming target by adjusting the ratio of light to a dark time [84]. In a PWM cycle, the brightness perceived by human eyes for light flicker greater than 100 Hz is a cumulative process. [85]. Therefore, the greater the proportion of bright time in

the entire cycle, the brighter the perceived illumination [86]. PWM provides high-quality white light, as well as a simple application and high efficiency [87] would be achieved. In addition to the EMI, another challenge with this dimming approach is the possibility for the LED driver to generate audible noise during operation.

In order to integrate VLC with PWM, the data duty cycle of the waveform can be adjusted utilizing a time-division multiplexing (TDM) scheme to transmit signals in [4]. In [88], subcarrier pulse position modulation (SC-PPM) and PWM are combined simultaneously to achieve dimming and transmitting data sequence.

In VLC systems, the large current spike will occur when the LEDs turn 'on', which will cause electromagnetic interference (EMI) [82] [89]. When PWM dimming is combined with VLC systems with large numbers of LEDs, EMI might be caused [89].

1.3.3 Spatial Dimming

Typical indoor lighting typically uses many LEDs to achieve sufficient brightness. In this way, multi-input multi-output (MIMO) communication system with multiple photo detectors (PDs) would be naturally formed at the receiver. Compared with traditional AD and DD technologies, spatial dimming (SD) is a more direct and effective dimming method considering spatial domain. The principle of spatial dimming technology is shown in Figure 1.7. As shown in Figure 1.7, for a luminaire with many LEDs, SD can achieve illumination level by activating part of LEDs working in the light source. So that signals in each LED would not be affected, which would avoid the loss of system communication rate. Subsequently, signals of the working LEDs will sum and be transmitted to the receiver in free-space as illustrated in Figure 1.7

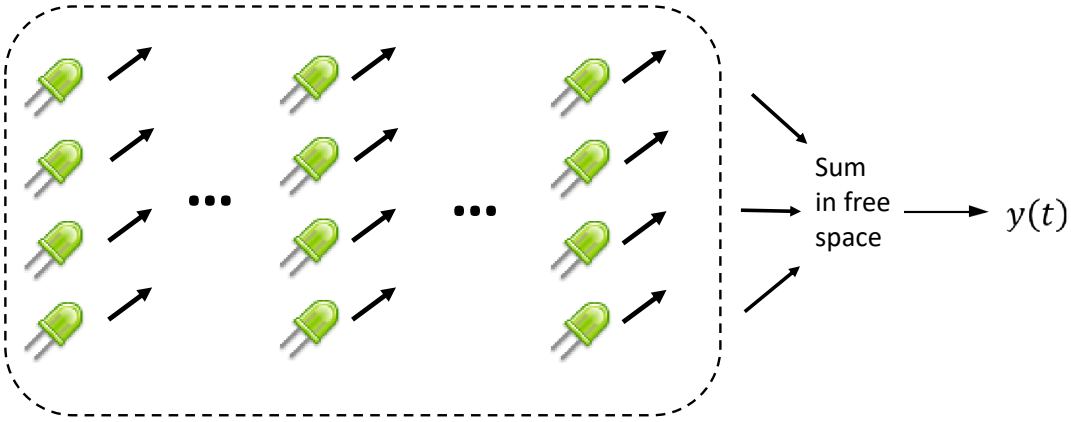

Figure 1.7: Principle of spatial dimming technology

where $y(t)$ is defined as the received signal.

At present, spatial dimming has been initially applied in the single-user visible light system. Reference [90] proposed the antennae basic boundary dimming (ASD) technology which uses the number of active LEDs to achieve the dimming target. ASD uses channel state information (CSI) to select the best antennae subset and achieve the highest channel gain [90]. In [91], Y. Yang proposed spatial dimming orthogonal frequency division multiplexing (SD-OFDM) technology which achieves dimming by changing the number of LEDs in the room. Owing to the fact that SD-OFDM technology does not change the DC bias of the signal, it significantly reduces the clipping noise of the signal compared to analogue dimming. It also keeps the signal in the 'on-state' during the dimming process, which can obtain a higher rate than digital dimming. Since the number of LEDs in the light source will limit the dimming accuracy of the system, the spatial dimming can jointly adjust the amplitude of the signal to achieve higher dimming accuracy.

1.3.4 Cooperation of VLC and dimming technology

Optical OFDM based VLC system with dimming is energy-efficient which adjusts the brightness of luminaires as different ambient light [92]. Two functions of VLC are illumination and communication [93], while the communication function of VLC systems may be influenced because of dimming.

As discussed in Section 1.2, DCO-OFDM and ACO-OFDM are two widely used OFDM techniques in VLC systems [94]. When digital dimming is integrated with DCO-OFDM, data-bearing signals are transmitted only in the 'on' states of corresponding PWM signals [94]. So when the dimming level is relatively low, most PWM

signals are in the 'off' state which cannot transmit data and ensure the communication quality. real-valued What is more, the performance of VLC systems will be impacted by clipping noise when the required dimming target is relatively high or low as discussed in Section 1.2.1 [69].

In VLC systems based on ACO-OFDM, the brightness of LEDs can be changed by signal and bias. The dynamic range for LEDs can be fully utilized when the dimming level is low [94] since the negative value of ACO-OFDM signals is clipped. While, if the dimming target for LEDs is high, the range where signals vary will shrink [94]. Therefore, the efficiency and quality of communication will be reduced.

Many other dimming schemes integrated with VLC systems are also proposed as follows. Y. Yang proposed Hybrid Dimming OFDM (HD-OFDM) technology in [51] where dimming accuracy and capacity of the system has been improved due to the simultaneous use of space and signal as resources. The main idea of HD-OFDM is to achieve a dimming target by DC bias and the number of working LEDs [51]. Spatial dimming adjusts the optical power by activating part of LEDs in lighting equipment to improve the communication performance of the system under different dimming targets [91].

However, the achievement of dimming function in VLC systems will directly affect the intensity of LEDs and the light source [95]. Hence, the performance of communication will be influenced by dimming control and then affect the number of transmitted bits in communication [96]. In this thesis, an optimal dimming scheme integrated with SO-OFDM is proposed to solve the problem of aforementioned dimming methods [51]. Proposed dimming methods based on VLC systems maximize the capacity of the system which maintains communication performance under different

illumination requirements.

1.4 Contributions of this Thesis

The main contribution of this thesis is to propose a novel power allocation scheme in spatial dimming which is based on spatial summing optical-OFDM (SO-OFDM) [2]. The traditional water pouring algorithm allocates the transmission power according to the channel conditions to maximize the transmission rate. Usually, when the channel conditions are good, more power will be allocated and when the channels are poor, less power will be allocated. The proposed scheme is based on SO-OFDM in [2] and combined with the water pouring scheme aiming to find the optical power allocation method for LEDs to not only meet the dimming requirements but also to maximize the communication rate of the VLC system. communication quality of the VLC system.

The developed water filling scheme allocates the transmission power to maximize the transmission rate and achieves the dimming target at the same time. Firstly, a non-convex problem is formed to calculate the capacity of SO-OFDM under a specified dimming target. Then this non-convex problem can be broken into a group of convex problems through approximations and constraint relaxation. The proposed scheme is solved by iteratively updating the clipping noise to achieve the optimal rate. The proposed scheme also agrees well with conventional water filling in which when the channel conditions are good, more power is allocated.

Numerical results and analytical results show that the proposed novel water filling scheme converges fast and performs well in different conditions.

1.5 Thesis Structure

The structure of the thesis is as follows. Chapter 2 describes the system model and channel model graphically, and the problem is stated. Chapter 3 discusses the proposed novel water pouring power allocation method for spatial dimming and communications. In addition, for different values of clipping noise, the power distribution method that maximizes the capacity of the system under group and subcarrier is discussed separately. Chapter 4 describes the simulation results of the system and compares the proposed power allocation method with allocating power uniformly. Chapter 5 summarizes the research work of the thesis and points out the direction of further research.

Chapter 2

System model

In this chapter, the system model of the SO-OFDM system and the spatial dimming block are illustrated. What is more, the channel model between LEDs and photo-detectors is also discussed with the explanation of parameters. Dimming constraints are stated so the problem is determining how to allocate power within constraints to optimize the performance of the system.

2.1 Spatial dimming Transmitter model based on SO-OFDM

As discussed in Section 1.2.2, the main idea of SO-OFDM is to separate a wideband input signal amongst subsets of carriers and emit them to different groups of LEDs [2]. In SO-OFDM, the setup of LEDs in G groups can be illustrated in Figure 2.1. In Figure 2.1, L and L_g represent the total number of LEDs and the number of LEDs for the g-th group separately. L LEDs are separated into G groups, so each group

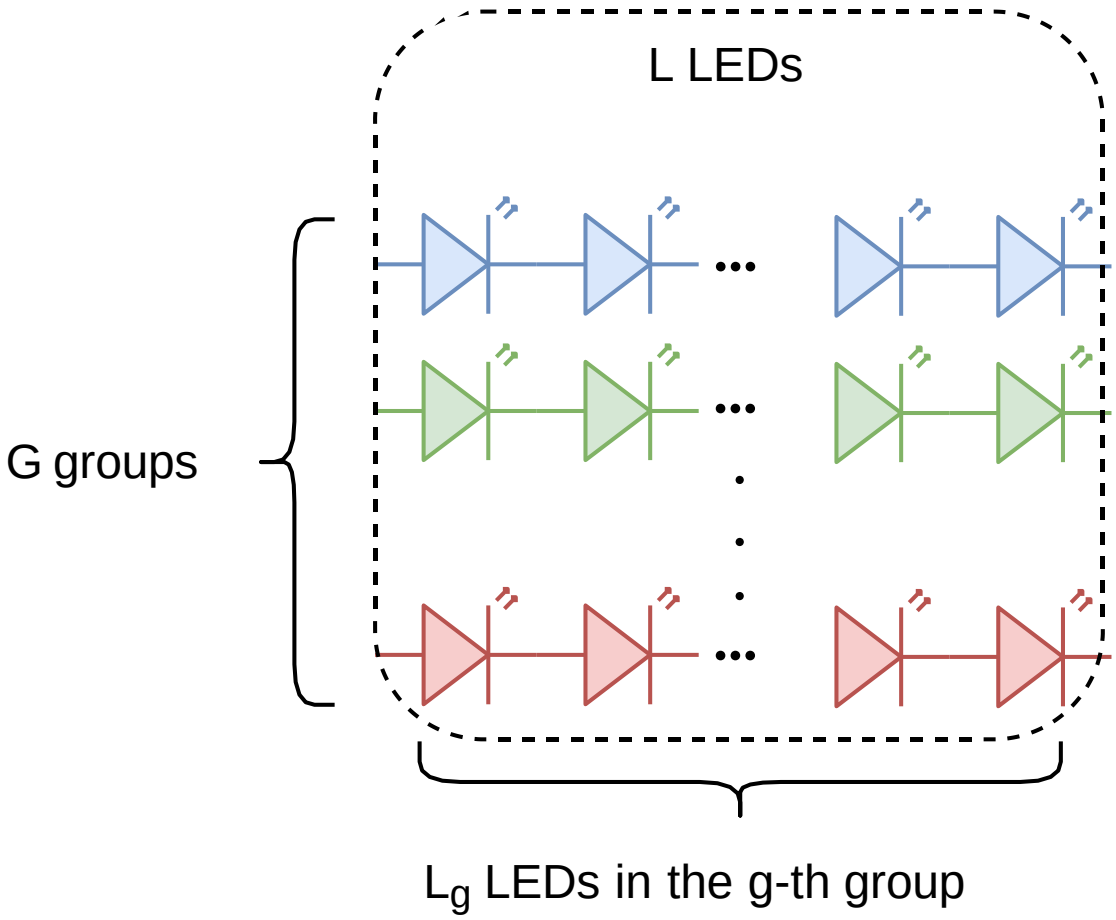

Figure 2.1: Setup of L LEDs in G groups for spatial summing in SO-OFDM

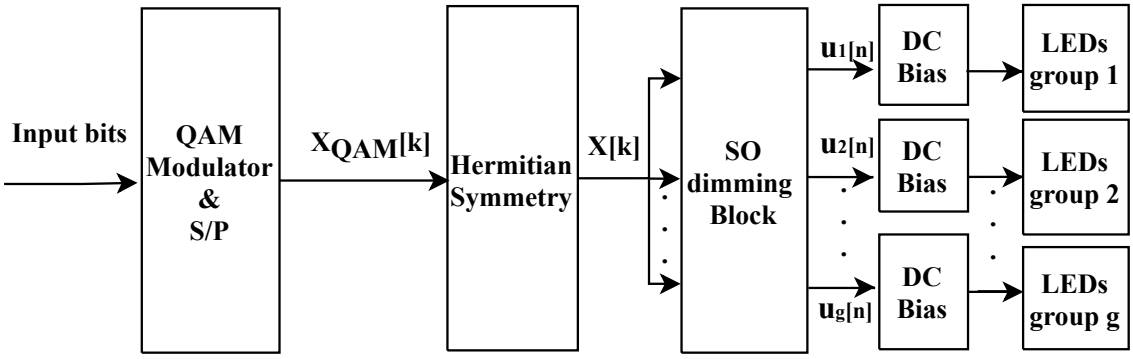

Figure 2.2: Architecture of spatial summing OFDM transmitter

has L_g LEDs where g ranges from 1 to G.

In VLC the concept of spatial summing means signals driving different LEDs are summed in space [2]. As discussed in Section 1.3.3, signals of those LEDs will sum in space during propagation in the optical wireless channel. Generally, the transmission delay and channel gain for different LEDs in the indoor VLC channel are different. However, the distance between each LED in each compact lamp is measured in centimetres, which is so negligible that the channel gains and delays of each LED can be supposed to be the same in our system [2].

Figure 2.2 describes the architecture of the proposed spatial dimming system which is based on SO-OFDM. The biggest difference between SO-OFDM and DCO-OFDM discussed in Section 1.2 is the spatial dimming block. The details of the spatial dimming block in Figure 2.2 are shown in Figure 2.3. Assume the number of total subcarriers is N where N is a power of 2. Considering Hermitian symmetry constraint, there are $N/2$ pairs of quadrature amplitude modulation (QAM) symbols, i.e., $X[k] = X^*[N-k]$ $(0 \leq k \leq N/2-1)$. $X[0]$ and $X[N/2]$ are set to zero which is similar to DCO-OFDM discussed in Section 1.2.1.

Allocating the wide band $N/2$ pairs of symbols among the G groups as shown in

Figure 2.3 such that in the g-th group there are narrow band $N_G/2$ pairs of symbols $X_g[k] = X_g^*[N-k]$ ($(g-1)N_G/2 \leq k \leq gN_G/2-1$, $N_G = N/G$) and the remaining subcarriers are set to zeros as in [2]. According to central limit theorem (CLT) [97], when N is large, the output of IFFT $x_g[n]$ in g-th group follows a Gaussian distribution with zero-mean and the variance σ_g^2.

Following Parseval's theorem, σ_g^2 is given by

$$\sigma_g^2 = \frac{2}{N}\sum_{k=0}^{N/2-1} \mathrm{E}\left[|X_g[k]|^2\right] = \frac{2}{N}\sum_{k=(g-1)N_G/2}^{gN_G/2-1} s_{g,k} \tag{2.1.1}$$

where

$$s_{g,k} \triangleq \mathrm{E}\left[|X_g[k]|^2\right] \tag{2.1.2}$$

i.e., the electrical power of the k-th channel in the g-th group.

As shown in Figure 2.3, assume $x_g[n]$ is hard symmetrically clipped to ensure that it is in the linear range of LEDs $[-I_{\mathrm{H},g}\ I_{\mathrm{H},g}]$ leading to [98]

$$u_g[n] = \begin{cases} I_{\mathrm{H},g}, & x_{\mathrm{g}}[n] > I_{\mathrm{H},g}, \\ x_g[n], & -I_{\mathrm{H},g} \leq x_g[n] \leq I_{\mathrm{H},g}, \\ -I_{\mathrm{H},g}, & x_g[n] < -I_{\mathrm{H},g}. \end{cases} \tag{2.1.3}$$

In the VLC system, transmitted time domain signals must be non-negative. After clipping $x_g[n]$, the following step is adding DC-bias $I_{\mathrm{DC,g}}$ for the clipped signals $u_g[n]$.

A DC bias $I_{\mathrm{DC},g}$ is added to $u_{\mathrm{g}}[n]$ to ensure that the signal is non-negative. Hence

$$I_{\mathrm{H},g} = \min\{I_{\mathrm{DC},g} - I_{\mathrm{L}}, I_{\mathrm{U}} - I_{\mathrm{DC},g}\}. \tag{2.1.4}$$

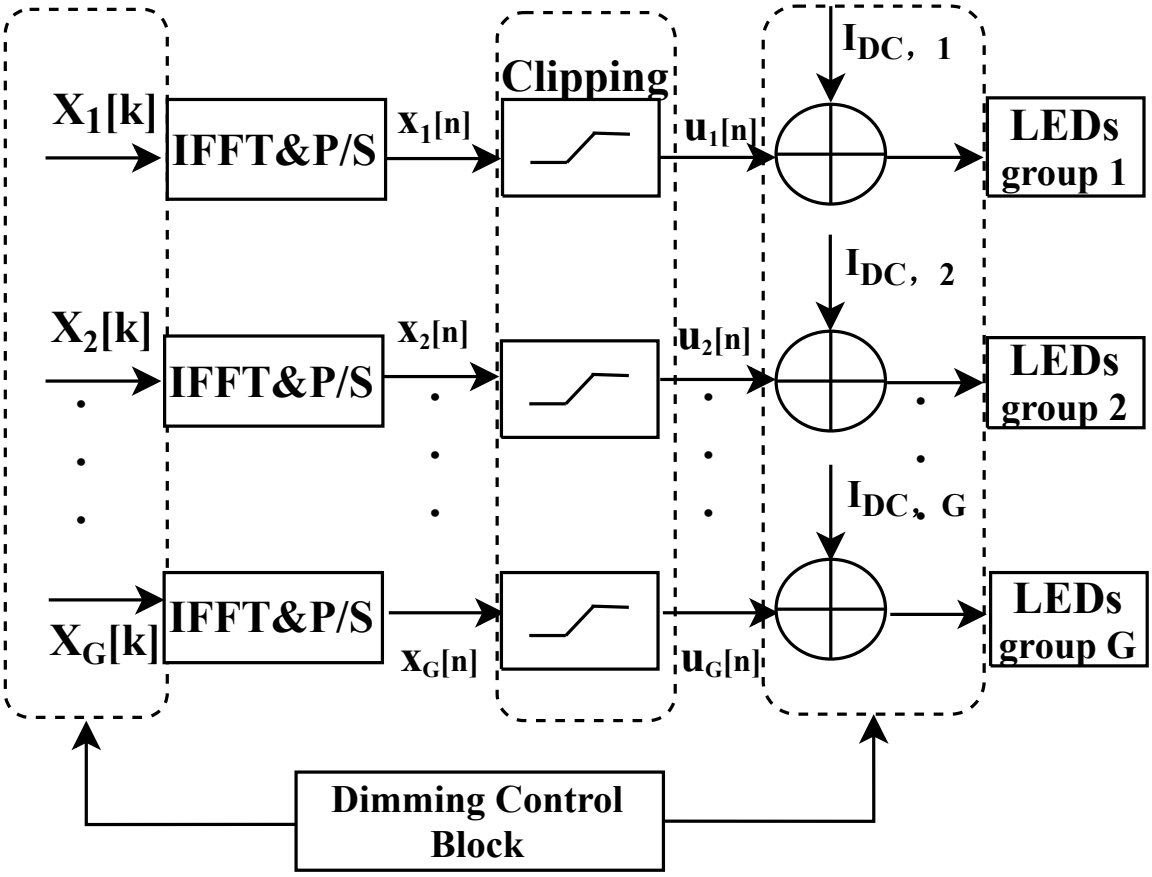

Figure 2.3: Block diagram of the spatial dimming block in the transmitter of SO-OFDM dimming system with G groups

Define

$$I_{\mathrm{H},g} = \mu\sigma_g = \mu\sqrt{\frac{2}{N}\sum_{k=(g-1)N_G/2}^{gN_G/2-1} s_{g,k}} \tag{2.1.5}$$

where μ is a proportional scalar in the g-th group corresponding to σ_g [2].

Rewriting (2.1.5) as an affine function with respect to $s_{g,k}$ as

$$\mu^2\frac{2}{N}\sum_{k=(g-1)N_G/2}^{gN_G/2-1} s_{g,k} = I_{\mathrm{H},g}^2, \quad g = 1,\ldots,G. \tag{2.1.6}$$

Finally, those clipped and biased signals from each group will drive the LEDs of each group accordingly. At the receiver, the received total optical power is converted to a photo-current by a photo-detector (PD) being corrupted by additive white Gaussian noise (AWGN), given by [99]

$$y[n] = G_{\mathrm{ele}}\sum_{g=1}^{G} L_g\left(u_g[n] + I_{\mathrm{DC,g}}\right) + z[n] \tag{2.1.7}$$

where G_{ele} is the electrical gain of the system. G_{ele} can be defined as

$$G_{\mathrm{ele}} = SG_{\mathrm{los}}R_{\mathrm{P}}, \tag{2.1.8}$$

where S denotes the LED conversion factor. G_{los} denotes the DC optical channel gain with line of sight (LOS) and R_{P} denotes the responsivity of the PD [2].

2.2 Channel Model

The LED emission pattern is assumed to have a Lambertian pattern [2]. Lambertian pattern refers to a radiation source that the radiant brightness of the source is constant

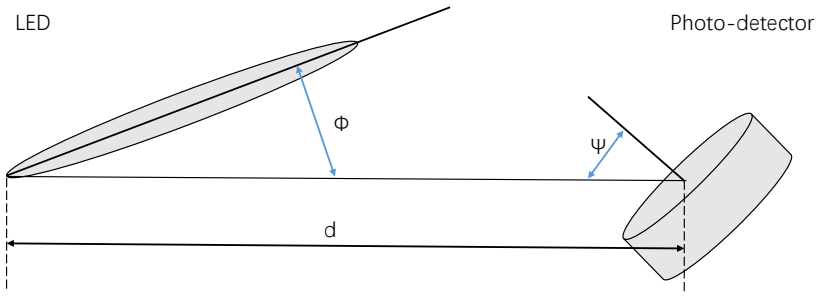

Figure 2.4: Diagram of LOS link [5]

in all directions [100].

At the receiver, a standard OFDM receiver is applied [2]. As justified precisely in this chapter, the distance between each LED is negligible. For the above reasons, we assume that the channel gain of a line of sight (LOS) between each LED and the photo-detector is equal [2]. The channel gain G_{los} can be written as [2]

$$G_{\text{los}} = \begin{cases} \frac{(m+1)A}{2\pi d^2} T_s(\psi) g(\psi) \cos^m(\phi) \cos(\psi), \text{ if } 0 < \psi < \Psi_c \\ 0, \text{ if } \psi > \Psi_c \end{cases}, \tag{2.2.1}$$

where m is the Lambertian order which is equal to $\frac{-\ln 2}{\ln\left(\cos \Phi_{1/2}\right)}$, $\Phi_{1/2}$ is the LED semi-angle at half illumination power, A is the area of detector. As shown in Figure 2.4, assume the LED emits an axially symmetric radiation [5], d is the distance between LED and the photo-detector, ϕ and ψ represent the angle of irradiance angle and

incidence angle respectively, ψ_c is the field of vision (FOV) for the receiver photo-detector, $T_s(\psi)$ and $g(\psi)$ are denotes as the gain of optical filter and the gain of optical concentrator respectively, where $g(\psi)$is given as [22]

$$g(\psi) = \begin{cases} \frac{n^2}{\sin^2 \Psi_c}, 0 \leq \psi \leq \Psi_c \\ 0, \quad 0 \geq \Psi_c \end{cases} \tag{2.2.2}$$

where n is the refractive index.

2.3 Dimming constraint

The illumination constraint and dimming are considered at the receiver plane in the thesis. Let P_{o} denote the total transmitted optical power from all the LEDs summed in space. $P_{\mathrm{o},g}$ is the transmitted optical power contributed by each LED in the g-th group. For convenience, $P_{\mathrm{o},g}$ and P_{o} are set to be unity in this thesis. We have

$$\sum_{g=1}^{G} L_g P_{\mathrm{o,g}} = P_{\mathrm{o}}. \tag{2.3.1}$$

Generally, $P_{\mathrm{o},g}$ is a linear function of the forward current [2] and

$$P_{\mathrm{o},g} = \mathrm{E}\left[S\left(u_g[n] + I_{\mathrm{DC,g}}\right)\right]. \tag{2.3.2}$$

According to (2.1.3), we have $\mathrm{E}\left[u_g[n]\right] = 0$ and plug this into (2.3.2) leading to

$$P_{\mathrm{o},g} = S I_{\mathrm{DC},g}. \tag{2.3.3}$$

Substituting (2.1.4) into (2.3.3),

$$S(I_{\mathrm{L}} + I_{\mathrm{H},g}) \leq P_{\mathrm{o},g} \leq S(I_{\mathrm{U}} - I_{\mathrm{H},g}). \tag{2.3.4}$$

Note that the illumination is a function of the luminaire and the illumination level is expected to be adjustable, i.e., dimming. Define $P_{\max}$ as the maximum total received optical power for illumination. Define dimming target α_{dim} as

$$\alpha_{\mathrm{dim}} = \frac{P_{\mathrm{o}}}{P_{\max}}, \tag{2.3.5}$$

where $\alpha_{\mathrm{dim}} = 1$ indicates full brightness with $P_{\mathrm{o}} = P_{\max}$.

It is worth noting that we can control $s_{g,k}$ and μ to achieve the required dimming target α_{dim} according to (2.1.4) and (2.3.3). According to (2.3.5), α_{dim} is a monotonically increasing function of P_{o} which is equal to the sum of $L_g P_{\mathrm{o,g}}$. Notice that $P_{\mathrm{o},g}$ is the function of $I_{\mathrm{DC},g}$ in (2.3.3) where $I_{\mathrm{DC},g}$ can be controlled by $I_{\mathrm{H},g}$ according to (2.1.4). In (2.1.5), $I_{\mathrm{H},g}$ is the function of $s_{g,k}$ and μ so that the dimming target can be achieved by adjusting $s_{g,k}$ and μ.

2.4 Summary

This chapter illustrates the system model of the SO-OFDM system and the channel model for each LED in the compact lamp can be seen as equal. The optimization problem will be solved in the next chapter according to those dimming constraints discussed in Chapter 2.

Chapter 3

Proposed Novel water pouring power allocation

In this chapter, the dimming of SO-OFDM is described as an optimization problem that is stated mathematically according to the system model described in Chapter 2. In order to solve the stated non-convex problem proposed in this chapter, a novel water pouring power allocation is proposed. The original problem is decomposed into two convex problems. Stated problems are solved in this chapter under different values of μ.

3.1 Problem statement

The architecture of spatial dimming OFDM is illustrated in Figure 3.1 where L LEDs are separated into G groups.

At the transmitter, QAM symbols from serial-to-parallel conversion are input to the Hermitian Symmetry and spatial dimming block to obtain the real time domain

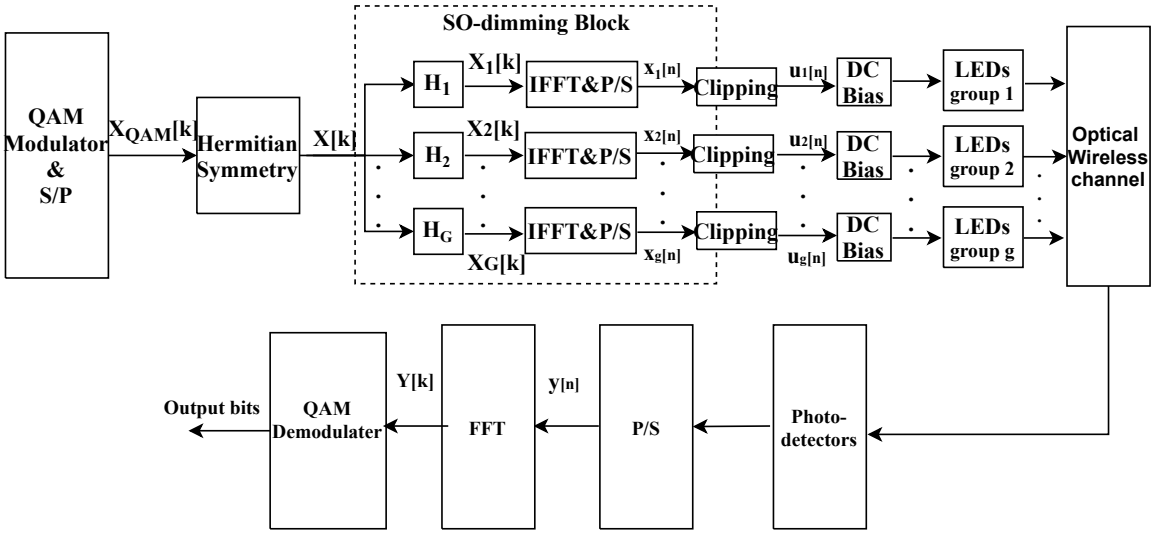

Figure 3.1: Block diagram of spatial dimming system with L_g LEDs in G groups [2]

.

clipped OFDM signal. As discussed in Chapter 2, assume that the number of total subcarriers is N. Due to Hermitian symmetry, there are only $\frac{N}{2}-1$ independent data carried subcarriers. According to central limit theorem (CLT) [97], when $X_{\mathrm{g}}[n]$ are added together and the number of subcarriers N is large enough (i.e., N is greater than 64), the distribution of $X_{\mathrm{g}}[n]$ can be seen as Gaussian distribution with zero-mean and variance σ_g^2,

$$\sigma_g^2 = \mathrm{E}\left[|x_{\mathrm{g}}[n]|^2\right] = \frac{2}{N}\sum_{k=1}^{N/2-1}\mathrm{E}\left[|X_g[k]|^2\right]. \tag{3.1.1}$$

In practice, as noted in [97], when the number of carriers is larger than 64 this Gaussian approximation is reasonable [97].

For the time domain signal $x_g[n]$ after taking the IFFT,

$$\begin{aligned} x_g[n] &= \frac{1}{\sqrt{N}} \sum_{k=0}^{N-1} X_g[k] \exp\left(\frac{j2\pi kn}{N}\right) \\ &= \frac{1}{\sqrt{N}} \sum_{k=1}^{N/2-1} \left\{ X_g[k] \exp\left(\frac{j2\pi kn}{N}\right) + X_g^*[k] \exp\left(-\frac{j2\pi kn}{N}\right) \right\} \\ &= \frac{2}{\sqrt{N}} \sum_{k=1}^{N/2-1} \Re\left\{ X_g[k] \exp\left(\frac{j2\pi kn}{N}\right) \right\} \\ &= \frac{2}{\sqrt{N}} \sum_{k=1}^{N/2-1} \left\{ \Re\left\{X_g[k]\right\} \cos\left(\frac{2\pi kn}{N}\right) - \Im\left\{X_g[k]\right\} \sin\left(\frac{2\pi kn}{N}\right) \right\} \end{aligned} \tag{3.1.2}$$

Signals from IFFT and P/S block are clipped to fit the dynamic range of LEDs. The clipped signal for each group $u_g[n]$ can be approximated using Bussgang's theorem [101]. This linear regression model of clipping for (2.1.3) can be rewritten as [99]

$$u_g[n] = K_g x_g[n] + c_g[n] \tag{3.1.3}$$

where $c_g[n]$ is clipping noise which is modelled as being uncorrelated with $x_g[n]$ [99] and K_{g} is a scalar. Meanwhile, the clipping noise term $c_g[n]$ in (2.1.3) should satisfy [2]

$$\mathbf{E}\left[x_g[n] c_g[n]\right] = 0.$$

Define γ_g as the clipping factor which is inversely proportional to the severity of the clipping distortion

$$\gamma_g \triangleq \frac{I_{\mathrm{H},g}}{\sqrt{2}\sigma_g} = \frac{\mu}{\sqrt{2}}. \tag{3.1.4}$$

The scalar K_{g} in (3.1.3) is a function of γ_g given by [99]

$$K_{\mathrm{g}} = \frac{\mathrm{Cov}[x(m), y(m)]}{\sigma_g^2} = \mathrm{erf}\left(\gamma_g\right) = 1 - \mathrm{erfc}\left(\gamma_g\right), \tag{3.1.5}$$

where

$$\mathrm{erf}(x) = \frac{2}{\sqrt{\pi}} \int_0^x \exp\{-t^2\}\mathrm{d}t. \tag{3.1.6}$$

The clipped signal $u_g[n]$ will have a DC bias I_{DC} added to ensure the non-negative of signals to drive LEDs.

At the receiver, the photo-detector receives the optical power from all LEDs. As discussed in Chapter 2, the intensities of LED sum in free space and the generated photo-current $y[n]$ can be modeled as

$$\begin{aligned} y[n] &= G_{\mathrm{ele}} \sum_{g=1}^{G} L_g y_g[n] + z[n] \\ &= G_{\mathrm{ele}} \sum_{g=1}^{G} L_g \left(u_g[n] + I_{\mathrm{DC}}\right) + z[n] \\ &= G_{\mathrm{ele}} \left[K_{\mathrm{g}} \sum_{g=1}^{G} L_g x_g[n] + \sum_{g=1}^{G} L_g c_g[n] + L_g \sum_{g=1}^{G} I_{\mathrm{DC}}\right] + z[n] \\ &= G_{\mathrm{ele}} \frac{L}{G} \left[K_{\mathrm{g}} \sum_{g=1}^{G} x_{\mathrm{g}}[n] + \sum_{g=1}^{G} c_g[n] + G I_{\mathrm{DC}}\right] + z[n]. \end{aligned} \tag{3.1.7}$$

where I_{DC} is the DC bias discussed in Chapter 2 as shown in Figure 3.1 and $z[n]$ is the additive white Gaussian noise (AWGN) term given as

$$z[n] \sim N\left(0, \sigma_z^2\right). \tag{3.1.8}$$

Since the DC bias carries no information, when the useful power of the system is calculated, the DC bias part is ignored.

The discrete Fourier transform (DFT) of the received signal in (3.1.7) with DC bias removed is

$$Y[k] = G_{\text{ele}} \sum_{g=1}^{G} L_g K_{\text{g}} X_{\text{g}}[k] + G_{\text{ele}} \sum_{g=1}^{G} L_g C_g[k] + Z[k], \tag{3.1.9}$$

where $C_g[k] = \text{DFT}\{c_g[n]\}$ is clipping noise and $Z[k] \sim \mathcal{N}(0, \sigma_{\text{z}}^2[k])$ is equivalent receiver noise. Assuming that the channels are equalized by a single tap complex multiplication. The model of (3.1.9) arises by considering an equalizer at the receiver. Assuming that the channels are equalized by a single tap complex multiplication. The equivalent noise with variance $\sigma_{\text{z}}^2[k] = \sigma_0^2/|H[k]|^2$, where σ_0^2 is AWGN and $H[k]$ is channel gain at the k th subcarrier.

Each data-bearing subcarrier discussed in Chapter 2 is allocated to a single group only, the useful power of symbol in the kth subcarrier in (3.1.9) can be defined as

$$\sigma_{\text{useful}}^2[k] = G_{\text{ele}}^2 \sum_{g=1}^{G} L_g^2 K_g^2 s_{g,k}. \tag{3.1.10}$$

The second term in (3.1.9) denotes clipping noise in the kth subcarrier, which is well modelled as AWGN based on CLT.

Theorem 1. *The variance of the clipping noise in each data-bearing subcarrier is same and in kth subcarrier is given by*

$$\sigma_{clip}^2[k] = G_{\text{ele}}^2 \sum_{g=1}^{G} L_g^2 \sigma_g^2 \Gamma(\gamma_g) \tag{3.1.11}$$

where for readability $\Gamma(\gamma_g)$ *is defined as the function of* γ_g *as*

$$\Gamma\left(\gamma_g\right) \triangleq \Big(\operatorname{erf}\left(\gamma_g\right) - \operatorname{erf}^2\left(\gamma_g\right) + 4\gamma_g^2\left(1 - \operatorname{erf}\left(\gamma_g\right)\right) - \tfrac{2\gamma_g}{\sqrt{\pi}} \exp\left(-\gamma_g^2\right)\Big) \tag{3.1.12}$$

Proof. For gth group, based on (3.1.3),

$$\mathrm{E}\left\{c_g[n]\right\} = \mathrm{E}\left\{u_g[n]\right\} - K_g \mathrm{E}\left\{x_g[n]\right\} = 0. \tag{3.1.13}$$

Considering the definition of DFT,

$$\mathrm{E}\left\{C_g[k]\right\} = \mathrm{E}\left\{c_g[n]\right\} = 0. \tag{3.1.14}$$

Hence, the variance of total clipping noise in the k th subcarrier from all the G groups is

$$\sigma^2_{\text{clip}}[k] = G^2_{\text{ele}} \sum_{g=1}^{G} L_g^2 \mathrm{E}\left\{\left|C_g[k]\right|^2\right\}. \tag{3.1.15}$$

Following the Parseval's theorem,

$$\mathrm{E}\left\{\left|C_g[k]\right|^2\right\} = \mathrm{E}\left\{\left|c_g[n]\right|^2\right\}. \tag{3.1.16}$$

Furthermore, based on (3.1.3) and (3.1.14),

$$\begin{aligned} &\mathrm{E}\left\{c_g[n]\right\}^2 = \mathrm{E}\left\{u_g^2[n]\right\} - K_{\mathrm{g}}^2\sigma_g^2 - 2\mathrm{E}\left\{c_g[n]\right\} K_{\mathrm{g}}\sigma_g \\ &= \mathrm{E}\left\{u_g^2[n]\right\} - K_{\mathrm{g}}^2\sigma_g^2 \\ &= \sigma_g^2\Big(\operatorname{erf}\left(\gamma_g\right) - \operatorname{erf}^2\left(\gamma_g\right) + 4\gamma_g^2(1 - \operatorname{erf}\left(\gamma_g\right)) - \frac{2\gamma_g}{\sqrt{\pi}} \exp\left(-\gamma_g^2\right)\Big). \end{aligned} \tag{3.1.17}$$

Substituting (3.1.16) into (3.1.15) leads to Theo. 1, where

$$\mathrm{E}\left\{u_g^2[n]\right\} = \sigma_g^2 \operatorname{erf}\left(\frac{c}{\sqrt{2}\sigma_g}\right) + c^2 \operatorname{erfc}\left(\frac{c}{\sqrt{2}\sigma_g}\right) - \frac{2\sigma_g c}{\sqrt{2\pi}} \exp\left(-\frac{c^2}{2\sigma_g^2}\right). \tag{3.1.18}$$

The proof of equation (3.1.18) is shown in the Appendix B. □

The performance of the proposed spatial dimming system is affected by clipping noise and the channel. For each subcarrier, the signal-to-noise-and-distortion ratio (SNDR) of k-th subcarrier is influenced by not only the useful power $\sigma^2_{\text{useful}}[k]$ but also AWGN noise $\sigma^2_{\text{z}}[k]$ and clipping distortion noise $\sigma^2_{\text{clip}}[k]$ [2]. The SNDR of the k-th subcarrier can be written as

$$\text{SNDR}[k] = \frac{\sigma^2_{\text{useful}}[k]}{\sigma^2_{\text{z}}[k] + \sigma^2_{\text{clip}}[k]}, \tag{3.1.19}$$

where $\sigma^2_{\text{useful}}[k]$, $\sigma^2_{\text{z}}[k]$ and $\sigma^2_{\text{clip}}[k]$ are defined in Section (3.1).

The bit error rate (BER) can be approximated for different square M-QAM modulation formation which can be estimated using the signal-to-noise-and-distortion ratio (SNDR) [2]. For each subcarrier, the bit error ratio for the subcarrier can be approximated as [102] [103]

$$\begin{aligned}\text{BER}[k] =& \frac{4(\sqrt{M}-1)}{\sqrt{M\log_2(M)}} Q\left(\sqrt{\frac{3\log_2(M)}{M-1}(\text{SNDR}[k])}\right) \\ &+ \frac{4(\sqrt{M}-2)}{\sqrt{M\log_2(M)}} Q\left(3\sqrt{\frac{3\log_2(M)}{M-1}(\text{SNDR}[k])}\right).\end{aligned} \tag{3.1.20}$$

Given that there are $N/2-1$ data-carrying subcarriers, the average BER is obtained as

$$\mathrm{BER} = \frac{1}{N/2-1} \sum_{k=1}^{N/2-1} \mathrm{BER}[k]. \tag{3.1.21}$$

Employing Shannon formula and the chain rule for mutual information, the achievable information rate of $(\frac{N}{2}-1)$ independent data carried subcarriers in SO-OFDM can be approximated

$$\begin{aligned} C &= \sum_{k=1}^{\frac{N}{2}-1} \log_2 \left(1 + \frac{\sigma^2_{\text{useful}}[k]}{\sigma^2_{\text{z}}[k] + \sigma^2_{\text{clip}}[k]}\right) \\ &\overset{(a)}{=} \sum_{g=1}^{G} \sum_{k=(g-1)N_G/2}^{gN_G/2-1} \log_2 \left(1 + \frac{G^2_{\text{ele}} L^2_g K^2_g s_{g,k}}{\sigma^2_{\text{z}}[k] + \sigma^2_{\text{clip}}[k]}\right) \end{aligned} \tag{3.1.22}$$

where (a) is due to each data-bearing subcarrier is only allocated to one group as presented in Section 2.1.

The power allocated to each carrier determines the capacity of the system. Hence, to find the optimal $s_{g,k}$ and μ to achieve the dimming target defined in Chapter 2 and maximize the capacity at the same time, an optimization problem is formulated

as

$$\mathbf{P1}: \max_{s_{g,k},\mu} \quad C \tag{3.1.23a}$$

$$\text{s.t.} \quad \sum_{g=1}^{G} L_g P_{\mathrm{o},g} = \alpha_{\mathrm{dim}} P_{\max}, \tag{3.1.23b}$$

$$P_{\mathrm{o},g} = S I_{\mathrm{DC},g}, \tag{3.1.23c}$$

$$I_{\mathrm{H},g} = \min\{I_{\mathrm{DC},g} - I_{\mathrm{L}}, I_{\mathrm{U}} - I_{\mathrm{DC},g}\}, \tag{3.1.23d}$$

$$\mu^2 \frac{2}{N} \sum_{k=(g-1)N_G/2}^{gN_G/2-1} s_{g,k} = I_{\mathrm{H},g}^2, \tag{3.1.23e}$$

$$s_{g,k} \geq 0, \tag{3.1.23f}$$

$$\mu \geq 0, \tag{3.1.23g}$$

where (3.1.23a) is the capacity in (3.1.22), (3.1.23b) is because the sum of optical power for each group is equal to the total optical power. **P1** is not a convex problem because the objective is not a convex function of $s_{g,k}$ and μ.

3.2 Problem solution

The impact of clipping on BER depends on the channel noise but it can be controlled by selection of μ [104]. In this section, we solve the problem in two conditions: (**P1**) when μ is large (greater than 2) and (**P2**) when μ is small (less than 2). Clipping noise is considered negligible in (3.1.22) when μ is large.

3.2.1 Qualitative Analysis

To solve the optimization problem, **P1** should be qualitatively analyzed. According to Chapter 2, the time domain signal $x_g[n]$ after IFFT is hard symmetrically clipped to fit the dynamic range of LEDs. The clipper clips the part of the $x_g[n]$ beyond the dynamic range symmetrically. The resulting distribution after clipping is symmetric about the mean of the Gaussian distribution.

To make it clear how symmetric clipping denoted by (2.1.3) works, three cases are illustrated in Figure 3.2 as an example with the increasing of $I_{\mathrm{DC},g}$. The PDF of three cases with $I_{\mathrm{DC},g} = 100,\ 250,$ and 400 mA respectively under symmetric clipping are shown in Figure 3.2. Corresponding to these three cases, $\alpha_{\mathrm{dim}} = 0.2,\ 0.5,$ and 0.8 respectively.

Assume the Gaussian noise $\sigma_{\mathrm{z}}^2[k]$ is the same in all three cases. For Case 1 and Case 3, the value of linear range $I_{\mathrm{H},g}$ is the same and $I_{\mathrm{H},g} = 100$ mA such that the value of σ_g is equal.

Hence, according to Theo. 1, the value of $\sigma_{\mathrm{clip}}^2[k]$ is equal such that the capacity of both cases should also be equal according to (3.1.22). That is, the capacity is symmetric with respect to

$$I_{\mathrm{DC},g} = \frac{I_L + I_U}{2} \tag{3.2.1}$$

i.e., for any two cases with $I_{\mathrm{DC},g}$ and $I'_{\mathrm{DC},g} = I_L + I_U - I_{\mathrm{DC},g}$ respectively, the capacity of the both cases are equal according to (3.1.22). Since the available linear range

$$I_{\mathrm{H},g} = \frac{I_L + I_U}{2} = 250 \text{ mA} \tag{3.2.2}$$

in Case 2 is biggest such that there is more freedom room to be employed for the

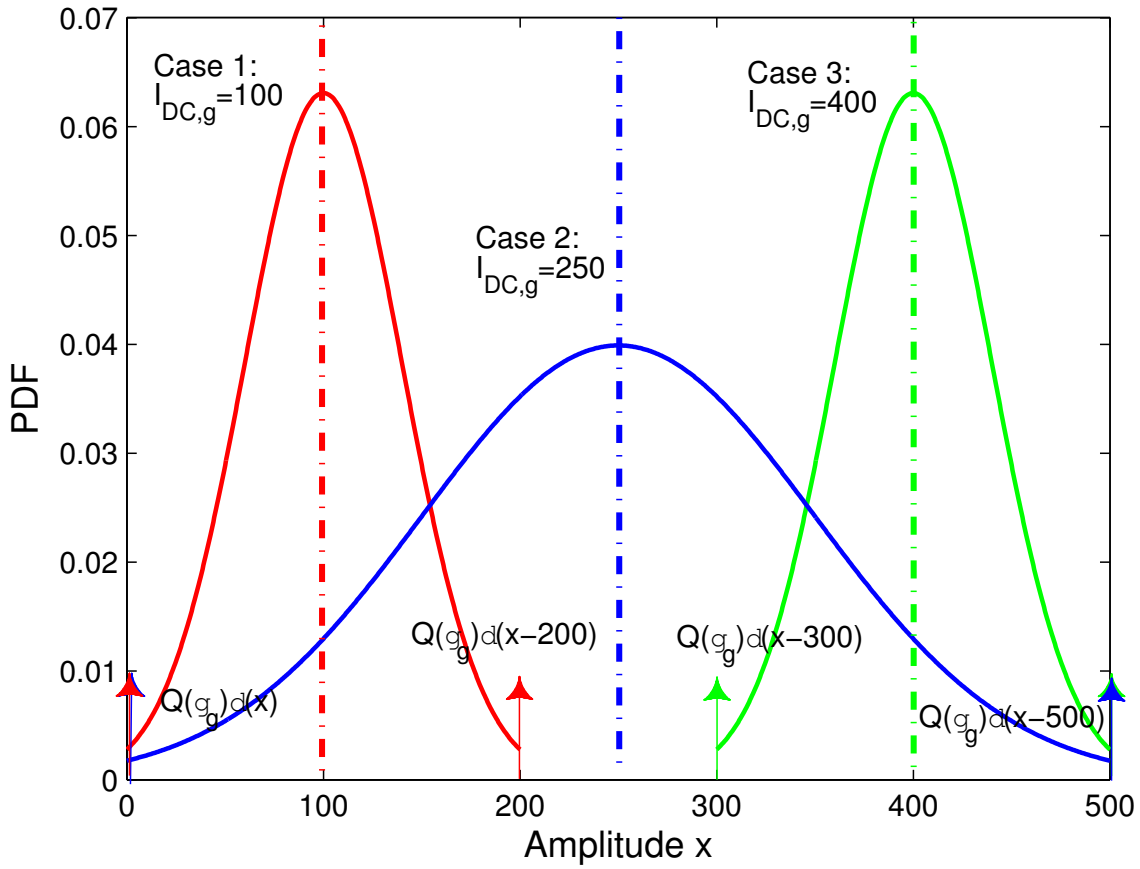

Figure 3.2: PDF of cases for different values of $I_{\mathrm{DC},g}$ and $I_{\mathrm{H},g}$ under symmetric clipping model in (2.1.3) ($I_l = 0$ mA, $I_u = 500$ mA, $\mu = 2.5$).

information carrying signal, the capacity should be maximum. It is safe to expect the capacity reaches maximum at

$$I_{\mathrm{H},g} = \frac{I_L + I_U}{2}. \tag{3.2.3}$$

As discussed in Section 3.1, **P1** is not a convex problem. Although $s_{g,k}$ and μ are not independent, μ can be treated as a parameter with a preset value and then solve **P1**.

Next, different values of μ are scanned and **P1** is solved under different values of μ. Finally, the capacity can be considered as the maximum rate under these different values of μ.

3.2.2 Problem P1: μ large

Firstly consider the case in which μ is large as discussed in Section 3.2 and there is no need to consider the clipping noise. In order to achieve the maximum value of the entropy, the input X_{i} should be independent and Gaussian distributed with variance optical power $I_{\mathrm{DC},g} = \mu\sigma_g$. $I_{\mathrm{DC},g}$ is added as a bias for the zero mean Gaussian process.

When choosing $I_{\mathrm{DC},g} = \mu \pm 3\sigma$, the area within $\mu \pm 3\sigma$ is 99.72% and the clipping noise is small [104]. So when μ is large, a reasonable assumption is to assume that the clipping noise is negligible, $\sigma^2_{\mathrm{clip}}[k] = 0$ in (3.1.22).

Hence, the objective (3.1.22) can be simplified to

$$C_{\mathrm{A}} = \sum_{g=1}^{G} \sum_{k=(g-1)N_G/2}^{gN_G/2-1} \log_2\left(1 + \frac{G^2_{\mathrm{ele}} L_g^2 K_g^2 s_{g,k}}{\sigma^2_{\mathrm{z}}[k]}\right). \tag{3.2.4}$$

In order to solve the non-convex problem, C_{A} is simplified to the convex problem C_{B}:

Theorem 2. *C_B is less than or equal to C_A where*

$$C_B = \sum_{g=1}^{G} \log_2 \left(1 + \frac{G_{\mathrm{ele}}^2 L_g^2 K_g^2 S_g}{\sigma_{z,g}^2} \right) \tag{3.2.5}$$

where

$$S_g \triangleq \sum_{k=(g-1)N_G/2}^{gN_G/2-1} s_{g,k} \tag{3.2.6}$$

and

$$\sigma_{z,g}^2 \triangleq \sum_{k=(g-1)N_G/2}^{gN_G/2-1} \sigma_z^2[k]. \tag{3.2.7}$$

Proof.

$$\begin{aligned} C_{\mathrm{A}} &= \sum_{g=1}^{G} \sum_{k=(g-1)N_G/2}^{gN_G/2-1} \log_2 \left(1 + \frac{G_{\mathrm{ele}}^2 L_g^2 K_g^2 s_{g,k}}{\sigma_{\mathrm{z}}^2[k]} \right) \\ &= \sum_{g=1}^{G} \log_2 \prod_{k=(g-1)N_G/2}^{gN_G/2-1} \left(1 + \frac{G_{\mathrm{ele}}^2 L_g^2 K_g^2 s_{g,k}}{\sigma_{\mathrm{z}}^2[k]} \right) \\ &\overset{(a)}{\geq} \sum_{g=1}^{G} \log_2 \left(1 + \sum_{k=(g-1)N_G/2}^{gN_G/2-1} \frac{G_{\mathrm{ele}}^2 L_g^2 K_g^2 s_{g,k}}{\sigma_{\mathrm{z}}^2[k]} \right) \\ &\overset{(b)}{\geq} \sum_{g=1}^{G} \log_2 \left(1 + \frac{G_{\mathrm{ele}}^2 L_g^2 K_g^2 S_g}{\sigma_{\mathrm{z},g}^2} \right) \end{aligned} \tag{3.2.8}$$

where (a) is due to discarding the negligible value of the expansion (i.e., ignoring all cross terms) and (b) is due to $s_{g,k} \geq 0$ and

$$\sum_{k=(g-1)N_G/2}^{gN_G/2-1} \frac{s_{g,k}}{\sigma_{\mathrm{z}}^2[k]} \geq \frac{\sum_{k=(g-1)N_G/2}^{gN_G/2-1} s_{g,k}}{\sum_{k=(g-1)N_G/2}^{gN_G/2-1} \sigma_{\mathrm{z}}^2[k]}. \tag{3.2.9}$$

where (3.2.9) can readily be proved by mathematical induction in Appendix B.

□

Substituting (3.2.6) into (3.2.15),

$$S_g = \frac{N I_{\mathrm{H},g}^2}{2\mu^2}. \tag{3.2.10}$$

Substituting (3.2.10) into (3.2.5) leading to

$$C_{\mathrm{B}} = \sum_{g=1}^{G} \log_2 \left(1 + \frac{N G_{\mathrm{ele}}^2 L_g^2 K_g^2 I_{\mathrm{H},g}^2}{2\mu^2 \sigma_{\mathrm{z},g}^2}\right) = \sum_{g=1}^{G} \left(\log_2 \left(\sqrt{1 + \frac{N G_{\mathrm{ele}}^2 L_g^2 K_g^2 I_{\mathrm{H},g}^2}{2\mu^2 \sigma_{\mathrm{z},g}^2}}\right)^2\right). \tag{3.2.11}$$

C_{B} is not a concave function with respect to $I_{\mathrm{H},g}$. By adding all cross terms, C_{B} can be approximated as

$$\begin{aligned} \tilde{C}_{\mathrm{B}} &= \sum_{g=1}^{G} \log_2 \left(1 + \frac{\sqrt{N} G_{\mathrm{ele}} L_g K_g}{\sqrt{2}\mu} \frac{I_{\mathrm{H},g}}{\sigma_{\mathrm{z},g}}\right)^2 \\ &= \sum_{g=1}^{G} 2 \log_2 \left(1 + \frac{\sqrt{N} G_{\mathrm{ele}} L_g K_g}{\sqrt{2}\mu} \frac{I_{\mathrm{H},g}}{\sigma_{\mathrm{z},g}}\right). \end{aligned} \tag{3.2.12}$$

where $\tilde{C}_{\mathrm{B}}$ is the sum of concave function and thus is a concave function with respect to $I_{\mathrm{H},g}$.

Problem P1 can be approximately decomposed into a series of problems. Firstly, define the problem **P2** and **P2**-g. **P2** considers power allocation over groups. Once power allocation of groups is done, then **P2**-g considers the power allocation over

subcarrier inside the group where

$$\mathbf{P2}: \max_{I_{\mathrm{H},g}} \quad \tilde{C}_{\mathrm{B}} \tag{3.2.13a}$$

$$\text{s.t.} \quad \sum_{g=1}^{G} SL_g(I_{\mathrm{L}} + I_{\mathrm{H},g}) \leq \alpha_{\mathrm{dim}} P_{\max}, \tag{3.2.13b}$$

$$\alpha_{\mathrm{dim}} P_{\max} \leq \sum_{g=1}^{G} SL_g(I_{\mathrm{U}} - I_{\mathrm{H},g}) \tag{3.2.13c}$$

$$I_{\mathrm{L}} \leq I_{\mathrm{H},g} \leq I_{\mathrm{U}} \tag{3.2.13d}$$

and

$$\mathbf{P2}\text{-}g: \max_{s_{g,k}} \quad \sum_{k=(g-1)N_G/2}^{gN_G/2-1} \log_2\left(1 + \frac{G_{\mathrm{ele}}^2 L_g^2 K_g^2 s_{g,k}}{\sigma_{\mathrm{z}}^2[k]}\right) \tag{3.2.14a}$$

$$\text{s.t.} \quad \sum_{k=(g-1)N_G/2}^{gN_G/2-1} s_{g,k} = \frac{N I_{\mathrm{H},g}^2}{2\mu^2}, \tag{3.2.14b}$$

$$s_{g,k} \geq 0. \tag{3.2.14c}$$

For **P2**, the objective is concave and the constraints are affine, which can be easily solved. **P2**-g can be treated as a conventional water filling problem. Denote $s_{g,k}^*$ as the solutions to **P2**-g. In **P2** and **P2**-g,

$$I_{\mathrm{H},g} = \mu\sigma_g = \mu\sqrt{\frac{2}{N}\sum_{k=(g-1)N_G/2}^{gN_G/2-1} s_{g,k}} \tag{3.2.15}$$

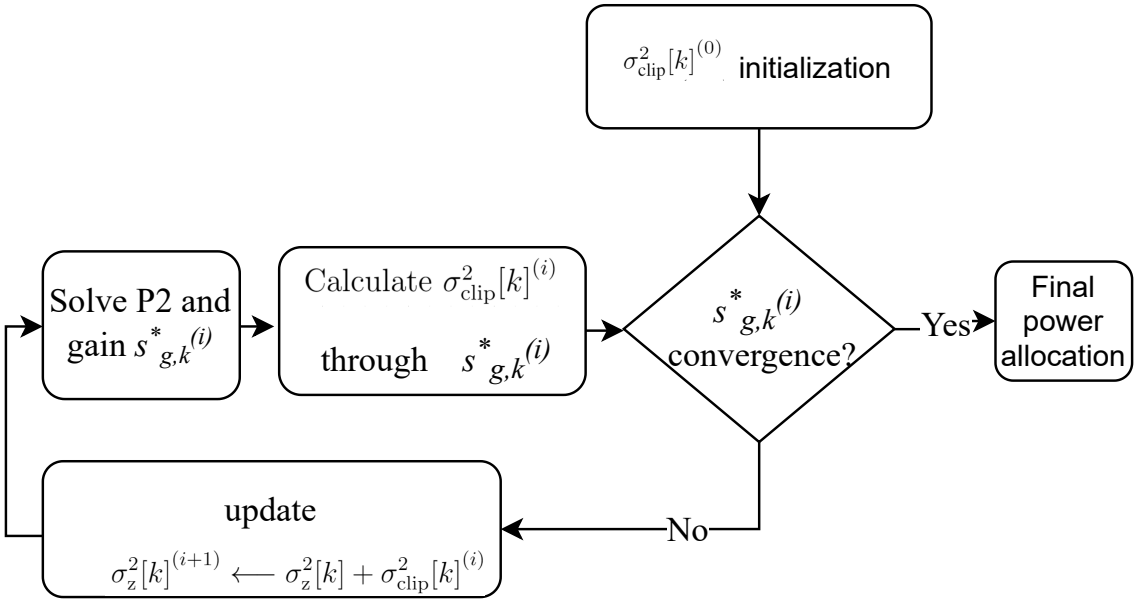

Figure 3.3: The flow chart of the proposed iteration approach to solve **P1** which applies to μ small case in Section 3.2.3

3.2.3 P1: μ small

When μ is small, the clipping noise is more severe. It is worth to note that in the frequency domain, the variance of the clipping noise in each data-bearing subcarrier is equal according to (3.1.11). This means the effect of clipping noise in each subcarrier is modelled as being the same.

Based on (3.1.22), when $\sigma^2_{\text{z}}[k] \gg \sigma^2_{\text{clip}}[k]$, the effect of AWGN noise dominates the power allocation; and when $\sigma^2_{\text{z}}[k] \ll \sigma^2_{\text{clip}}[k]$, the effect of clipping noise dominates the power allocation.

Based on the above analysis, an iterative approach is proposed to solve **P1**, and in one iteration the clipping noise is updated from the last iteration.

Specifically, define $\sigma^2_{\text{clip}}[k]^{(i)}$ and $s^*_{g,k}{}^{(i)}$ as the variance and the solutions to **P2**-g for i-th iteration. To achieve power allocation, considering the effect of clipping by

calculating $\sigma^2_{\text{clip}}[k]^{(i)}$ through ${s^*_{g,k}}^{(i)}$, and then in the $(i+1)$-th iteration update noise variance by

$$\sigma^2_{\text{z}}[k]^{(i+1)} \longleftarrow \sigma^2_{\text{z}}[k] + \sigma^2_{\text{clip}}[k]^{(i)}. \tag{3.2.16}$$

Again, updating ${s^*_{g,k}}^{(i+1)}$ by solving **P2** under $\sigma^2_{\text{z}}[k]^{(i+1)}$ and calculate $\sigma^2_{\text{clip}}[k]^{(i+1)}$ for $(i+2)$-th iteration. This iterative approach is summarized in Fig. 3.3. Hence, **P1** can be solved by this iterative approach when it finally converges or meets the maximum number of iterations. Convergence using this approach is not guaranteed, however, in practice (as seen in Chapter 4) this process does converge. Assume $S[k]$ is the final optimal average electrical power at the k-th subcarrier.

3.3 Summary

In this chapter, our proposed power allocation method under dimming target is described and optimized. Firstly, problems are stated under constraints discussed in Chapter 2 previously. When clipping noise is small and can be ignored, the objective (3.1.22) can be simplified. So that, according to the value of clipping noise, two different conditions are described with different values of μ. If μ is very large, the DC bias will be much bigger and the clipped part of the signal is so small that the influence of clipping noise in the SNR region can be ignored [99]. Furthermore, the situation should be considered when the clipping distortion is ignored. In this condition, the Bussgang theorem can be used to model the clipping noise and iteratively the clipping noise should be updated until achieving the optimal capacity.

Chapter 4

Simulation and Numerical Results

In this chapter, simulations are conducted to analyze the performance of the proposed spatial dimming scheme discuessed in Chapter 2 with power allocation defended according to Chapter 3. The simulation result shows that the proposed power allocation scheme performs well and the results match the conventional water filling philosophy.

4.1 Parameter Selection

This section mainly sets the parameters according to references and real world constraints. Assume that there are $N = 256$ subcarriers and $L = 8$ LEDs. For each LED, set $I_L = 0$ mA and $I_U = 500$ mA. In all analyses, the available bandwidth of each LED is $B = 100$ MHz [102] and the double-sided power spectral density of AWGN is $N_0/2 = 10^{-14}/2$ mA^2/Hz. Hence, σ_0^2 can be written as

$$\sigma_0^2 = BN_0 = 10^{-6}\text{mA}^2. \tag{4.1.1}$$

Parameters for the optical channel gain G_{los} mentioned in Chapter 2.2 are shown in Table 4.1. In the simulation, $P_{\max} = GL_gSI_{\text{U}}$ according to (2.3.1) and (2.3.2). For example, when $G = 4$ and $L_{\text{g}} = 2$, $P_{\max} = 16$W. The value of G_{ele} will nor influence power allocation since it is just a constant in our problem.

As discussed in Chapter 2, channel gains between each LED to the receiver is equal [2]. The channel gain of k-th subcarrier is given by [105] [106]

$$H[k] = 1/\sqrt{2}\exp((k - N/2)^2/(2\sigma_{\text{H}}^2 N^2)), \tag{4.1.2}$$

with $\sigma_{\text{H}}^2 = \frac{1}{4\ln 4}$ thus leads to a 6-dB cut off frequency, i.e.,

$$|H[N/2]|^2 = 0.25|H[0]|^2. \tag{4.1.3}$$

4.2 Simulation Results

In this section, simulation results are shown to analyze the performance of the proposed power allocation scheme with different group numbers G, dimming target α_{dim} and proportional scalar μ. Although μ is a fixed parameter, it must be properly selected to balance the impact of clipping and channel noise on the overall capacity. To explore the relationship between power allocation and channel gain, the power allocated for each subcarrier and the corresponding noise are also demonstrated in this part. The approximations are used only for design purposes. In later results, the calculation of the capacity using the exact expression (3.1.22) discussed in Chapter 3.

Table 4.1: Simulation Parameters [2] [7]

Symbol	Name of Parameters	Values
I_{H}	Maximum allowed current	2A
I_{L}	Minimum allowed current	0A
σ^2	The electrical power of the signal	1 W
$\Phi_{1/2}$	Semiangle at half power	60 [deg.]
$\mathrm{T_s}(\psi)$	Gain of the optical filter	1
n	Refractive index	1.5
A	Physical area of a PD	1[cm^2]
ψ_{c}	Receiver FOV semi-angle	80 [deg.]
d	Distance between the transmitter and receiver,	2m
ϕ	Angle of irradiance,	0 [deg.]
ψ	Angle of incidence,	0 [deg.]
$\mathrm{G_{ele}}$	line of sight,	1
S	LED conversion factor,	1W/A
$\mathrm{G_{los}}$	line of sight,	1
$\mathrm{R_P}$	responsivity of the PD,	1[A/W]

4.2.1 Iteration of clipping noise

In this part, the iteration of clipping noise with different situations is discussed. The purpose of this section is to show that the loop defined earlier converges. The optimization problems defined in Chapter 3 converge in practice for the practical values. In order to solve **P2** and **P2-***g* in Section (3.2), Matlab Software for Disciplined Convex Programming (CVX) is utilized [107] [108]. As illustrated in Section 3.2.3, **P2** can be solved by iterating on the resulting clipping noise.

Firstly, to find an optimized power distribution, the effect of clipping noise for each subcarrier is considered by calculating the variance of the clipping noise $\sigma^2_{\text{clip}}[k]^{(i)}$ according to (3.1.11) in Chapter 3. Then in the $(i+1)$-th iteration the noise variance is considered continuously until the clipping noise converges.

Figure 4.1 to Figure 4.4 illustrate the convergence of $\sigma^2_{\text{clip}}[k]^{(i)}$ as iteration number i increases, in which $G = 8$ is fixed for different μ and α_{dim}. It can be seen that the convergence of $\sigma^2_{\text{clip}}[k]^{(i)}$ is quickly in practice in our simulations. As shown in Figure 4.1 to Figure 4.4, $\sigma^2_{\text{clip}}[k]^{(i)}$ converges after the second iteration when $G = 8$. As discussed in Chapter 3 When μ is large (μ >2) and the clipping noise can be ignored, then the iteration time is 0 (i.e., no iteration is necessary). While when μ is small (μ <2), the clipping noise should be considered. The total iteration number i for $\sigma^2_{\text{clip}}[k]^{(i)}$ can be set as 3. The iteration of $s^{(i)}_{g,k}$ is illustrated in the Appendix B which also shows that the iteration number i set as 3 is reasonable.

4.2.2 Power allocation results

In this part, according to an optimized power allocation scheme. proposed in Section 3, the power allocated to each subcarrier with different conditions is displayed, and the

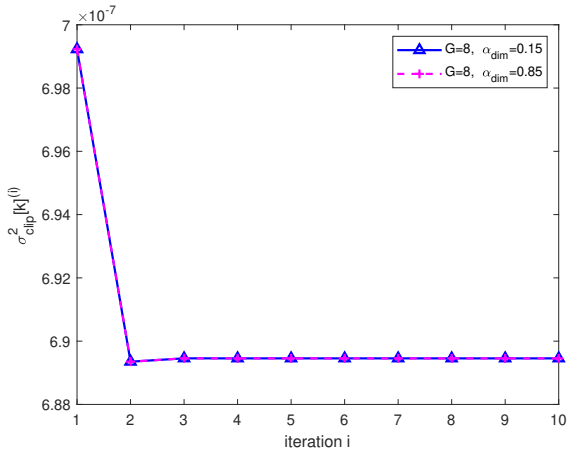

Figure 4.1: $\sigma^2_{\text{clip}}[k]^{(i)}$ vs iteration number i ($\mu = 1.5$, $\alpha_{\text{dim}} = 0.15$; $\alpha_{\text{dim}} = 0.85$ and $G = 8$).

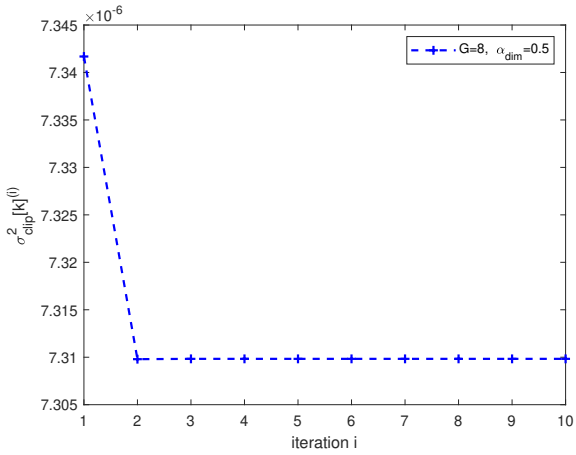

Figure 4.2: $\sigma^2_{\text{clip}}[k]^{(i)}$ vs iteration number i ($\mu = 1.5$, $\alpha_{\text{dim}} = 0.5$ and $G = 8$).

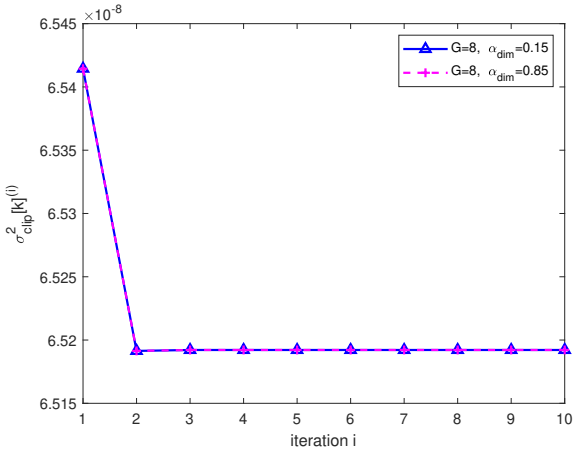

Figure 4.3: $\sigma^2_{\text{clip}}[k]^{(i)}$ vs iteration number i ($\mu = 2.5$, $\alpha_{\text{dim}} = 0.15$; $\alpha_{\text{dim}} = 0.85$ and $G = 8$).

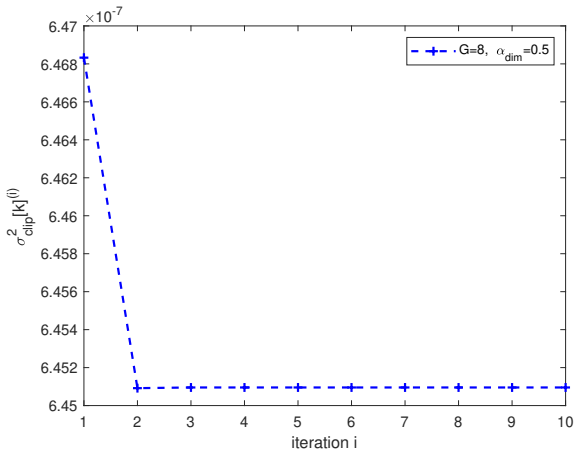

Figure 4.4: $\sigma^2_{\text{clip}}[k]^{(i)}$ vs iteration number i ($\mu = 2.5$, $\alpha_{\text{dim}} = 0.5$ and $G = 8$).

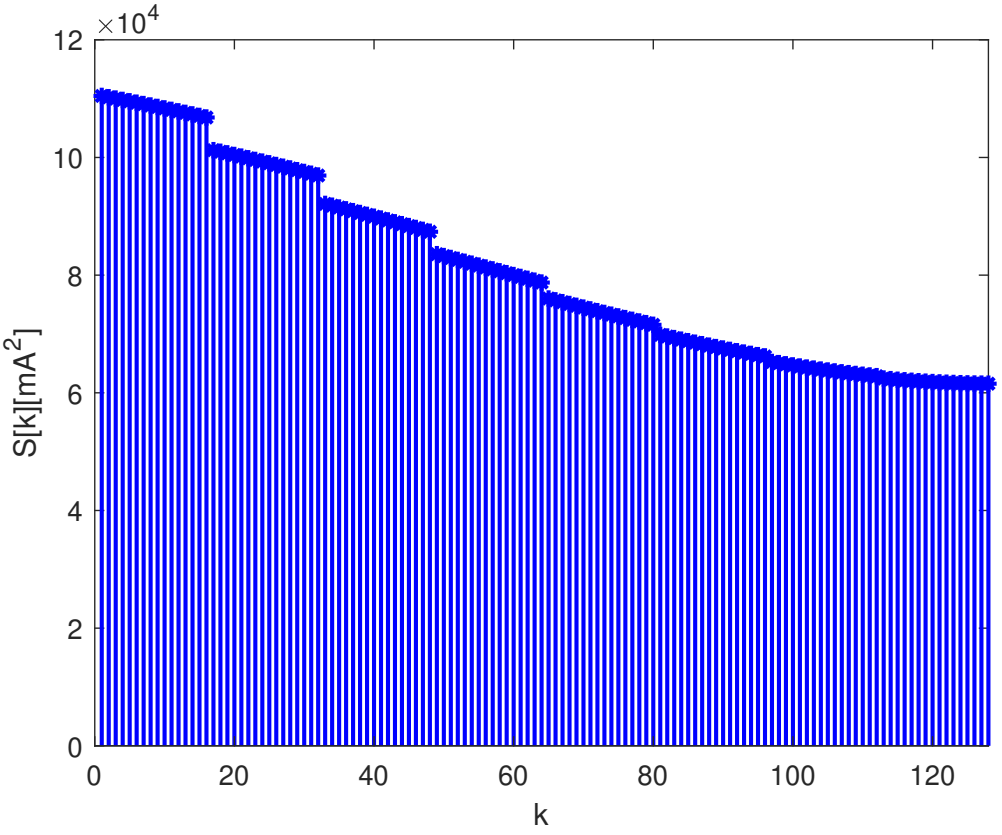

Figure 4.5: Distribution of symbol power $S[k]$ at each data-bearing subcarrier ($\mu = 2.5$, $\alpha_{\text{dim}} = 0.5$ and $G = 8$).

relationship between the power allocation of each subcarrier $S[k]$ and corresponding noise variance $\sigma_z^2[k]$ can also be compared. In the process of solving the optimal power allocation problem, CVX [109] and the clipping noise $\sigma_{\text{clip}}^2[k]^{(i)}$ in the previous section are utilized.

The distribution of symbol power $S[k]$ and noise variance $\sigma_z^2[k]$ at each data-carrying subcarrier are shown in Figure 4.5 and Figure 4.6, in which $\mu = 2.5$ with $\alpha_{\text{dim}} = 0.5$ and $G = 8$ are fixed.

In Figure 4.5 and Figure 4.6, the x-axis is the number of subcarriers where k refers

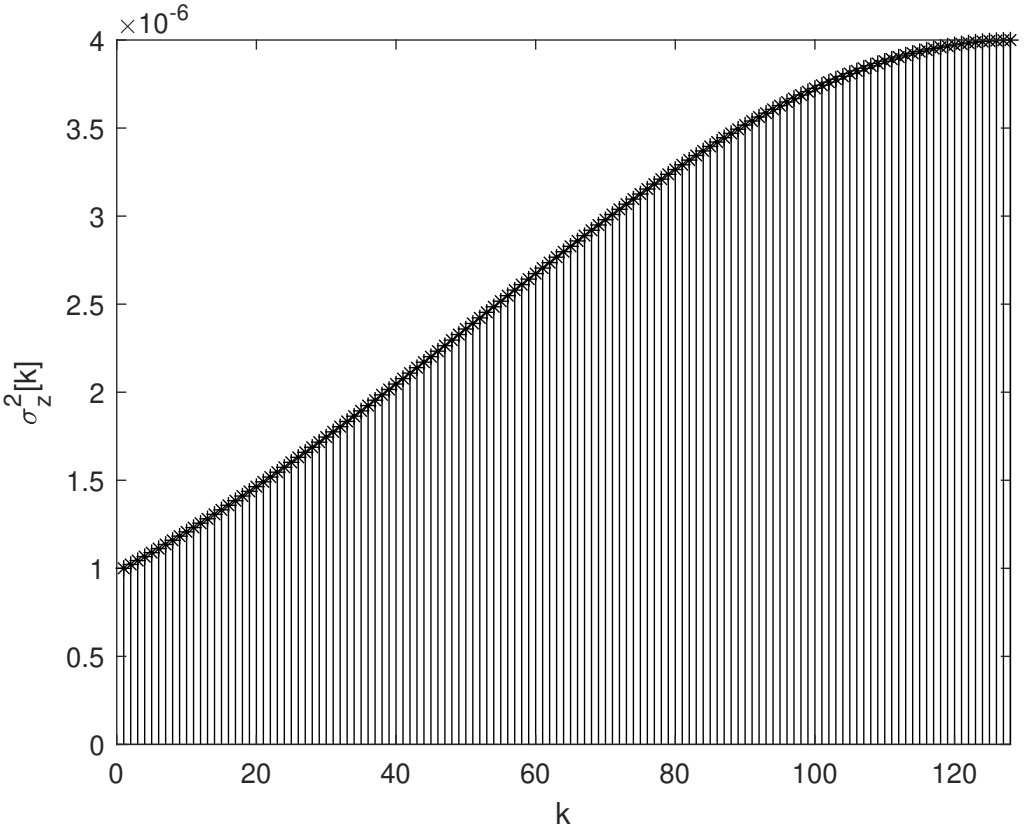

Figure 4.6: Distribution of channel noise variance $\sigma_z^2[k] = \sigma_0^2/|H[k]|^2$ at each data-bearing subcarrier (same condition with Figure 4.5
)

to the power of the k-th carrier. The y-axis of Figure 4.5 is the power allocated to each subcarrier and the y-axis for Figure 4.6 is the channel noise variance $\sigma_z^2[k]$ for k-th subcarriers. Similar to traditional water pouring, the proposed scheme will allocate more of the power to those subcarriers with low noise variance and small amounts of power to noisy subcarriers. This satisfies intuition as channels with favourable channel gains are allocated more power which matches the conventional water filling method mentioned in [110].

4.2.3 Simulation results of proposed system

For this part, the capacity of the system C in (3.1.22) is discussed according to the proposed optimal power allocation scheme. $\tilde{C}_{\mathrm{B}}$ and C_{B} are only defined to make an objective that is easily solved using the optimizer. The following simulation results in this part have selected the case of $G = 8$ and $\mu = 2.5$ for simulation. Corresponding capacity results and bit error rate for other cases are presented in the Appendix A.

The capacity (3.2.4) discussed in Chapter 3 for $G = 8$ with different dimming levels α_{dim} and different μ is shown in Figure 4.7. With the increasing of μ, there is a trade-off between clipping noise variance σ^2_{clip} and useful power $\sigma^2_{\mathrm{useful}}$. It can be seen that the capacity increases as the dimming target α_{dim} increases from 0 to 0.5. This is because the available linear range, $I_{H,g}$, of each LED modulating signal increases thus increasing the total available power. However, when α_{dim} keeps increasing from 0.5 to 1, the capacity will decrease due to the reduction of $I_{H,g}$ for LEDs to fit the dynamic range of each LED.

When $\alpha_{\mathrm{dim}} \leq 0.3$ or $\alpha_{\mathrm{dim}} \geq 0.7$, capacity with $\mu = 1.5$ is the largest. This is likely caused by the large clipping noise. The capacity when $\mu = 2.5$ is largest

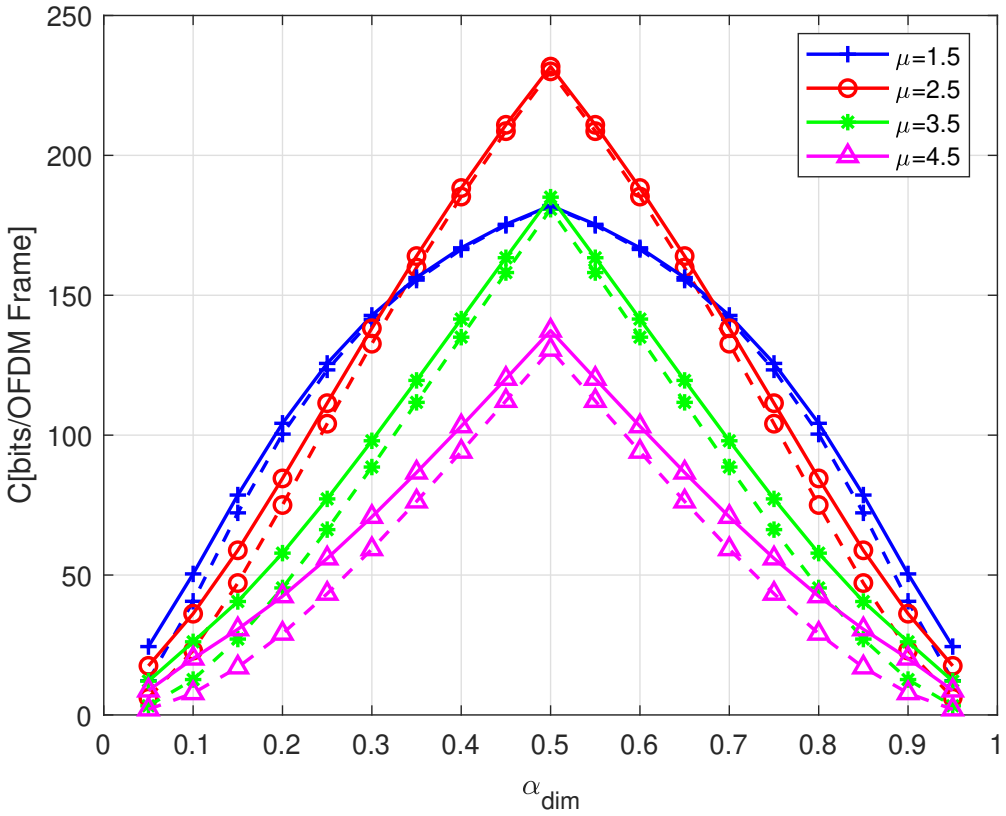

Figure 4.7: Capacity of SO-OFDM for different dimming levels with $G = 8$ group (Solid lines show results by solving **P2** and dot lines uniformly distributed $S[k]$).

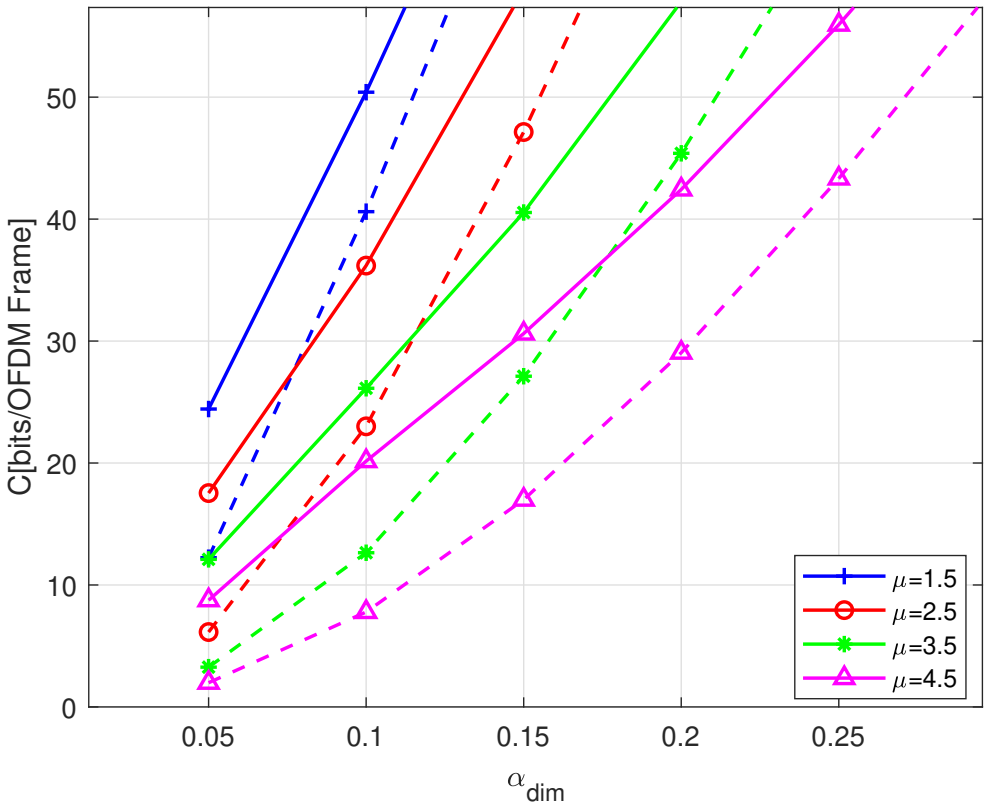

Figure 4.8: Zoomed-in-figure for Figure 4.7 (Solid lines show results by solving **P2** and dot lines uniformly distributed $S[k]$).

with $0.3 \leq \alpha_{\text{dim}} \leq 0.7$ and reaches the peak when $\alpha_{\text{dim}} = 0.5$ because clipping noise is reduced as μ increases. If μ continues to increase to 3.5 or 4.5, the capacity will reduce, since increasing μ causes a reduction in $\sigma^2_{\text{useful}}[k]$ in (3.1.10) as well. Furthermore, the capacity is symmetric with respect to $\alpha_{\text{dim}} = 0.5$ and reaches its maximum at $\alpha_{\text{dim}} = 0.5$ as discussed in Section 3.2.

The achievable information rate with uniformly distributed power denoted by dot lines is also shown in Figure 4.7 as a reference. The power allocated to each subcarrier can be calculated as

$$s_{g,k,\text{uniform}} = \frac{N I^2_{\text{H},g}}{N_G \mu^2} \tag{4.2.1}$$

where $I_{\text{H},g} = \min\{I_{\text{U}} - \frac{\alpha_{\text{dim}} P_{\max}}{GSL_g}, \frac{\alpha_{\text{dim}} P_{\max}}{GSL_g} - I_{\text{L}}\}$ according to (3.2.13b),(3.2.13c), (3.2.13d) and (3.2.14b).

Compared to the rate with the uniform power allocation, the capacity obtained by solving **P2** is larger when α_{dim} is small. This is because when α_{dim} is small, SNR is also small and channel noise has a large effect on the power allocation among data-bearing subcarriers. When α_{dim} is large, the channel noise is relatively small as compared to the signal power.

The details of the channel capacity where α_{dim} ranges from 0.05 to 0.3 are shown in Figure 4.8 which is the zoomed-in-figure of Figure 4.7. In Figure 4.7, when α_{dim}=0.1, the capacity of the proposed power allocation method is about twice of the capacity for uniform distribution. When α_{dim} is less than 0.5, with the increase of α_{dim}, the gap of channel capacity for the optimal power allocation scheme and the uniform distribution scheme becomes smaller. This is because when the total power is small, the limited power should be allocated optimally to obtain a larger capacity. However, when the dimming target is large enough, the power is large enough to allocate for

each subcarrier, the gap between the optimal power distribution scheme and the uniform power distribution scheme will become smaller. These phenomena also agree well with conventional water filling in the high SNR regime.

Furthermore, a flat channel with noise variance $\sigma_z^2[k]$ is equal at each data-carrying subcarrier shown in Figure 4.10, in which $\mu = 2.5$ and $G = 8$. In this condition, the performance of the proposed power allocation scheme and uniform power allocation scheme can be observed in Figure 4.9. In Figure 4.9, the red solid line represents the channel capacity with the optimal power allocation scheme and the blue dashed line represents the channel capacity with the average power allocation scheme. As shown in the figure, these two lines coincide with each other. This is because the channel is flat, and the noise variance $\sigma_z^2[k]$ corresponding to each subcarrier is the same, so the optimal power allocation scheme is the same as the average power allocation scheme. It also verifies that the previous analysis is correct.

These phenomena when $G = 8$ also agree well with simulation results in Section 4.2. For all of these results, the proposed power allocation scheme always performs well. For example, as shown in Figure 4.7, the information rate with the proposed power allocation scheme is exceeds twice the information rate with the uniform power loading when $\alpha_{dim} < 0.15$ or $\alpha_{dim} > 0.85$ with $G = 8$ and $\mu = 4.5$.

To summarize, the power allocation of the proposed system can be calculated by solving **P2**. With the increasing dimming target, μ can be selected according to the results of the performance. For example, when α_{dim} is small ($\alpha_{dim} < 0.3$), μ can be selected as 1.5 when $G = 8$ according to Figure 4.7. The transmitted power can be allocated according to the result of the solution of **P2**. While, when α_{dim} is large enough (such as when α_{dim}=1), the corresponding transmitted power is also large.

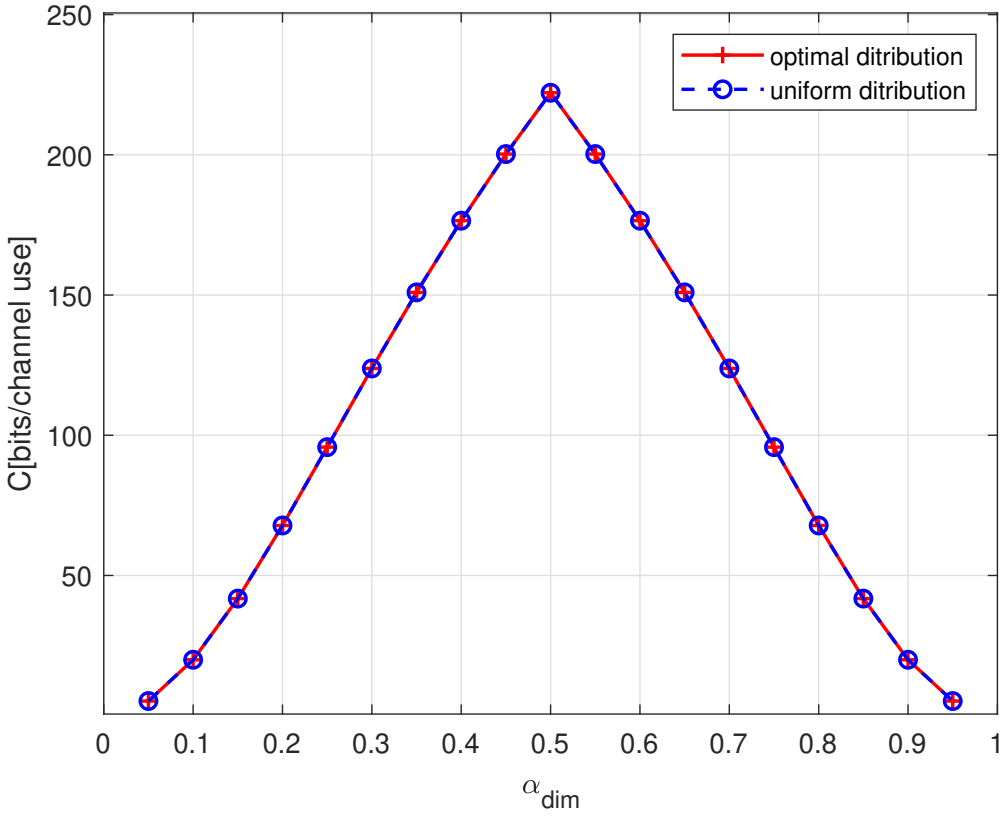

Figure 4.9: Capacity of SO-OFDM for different dimming levels with $G = 8$ groups in flat channel (Solid lines show results by solving **P2** and dot lines uniformly distributed $S[k]$).

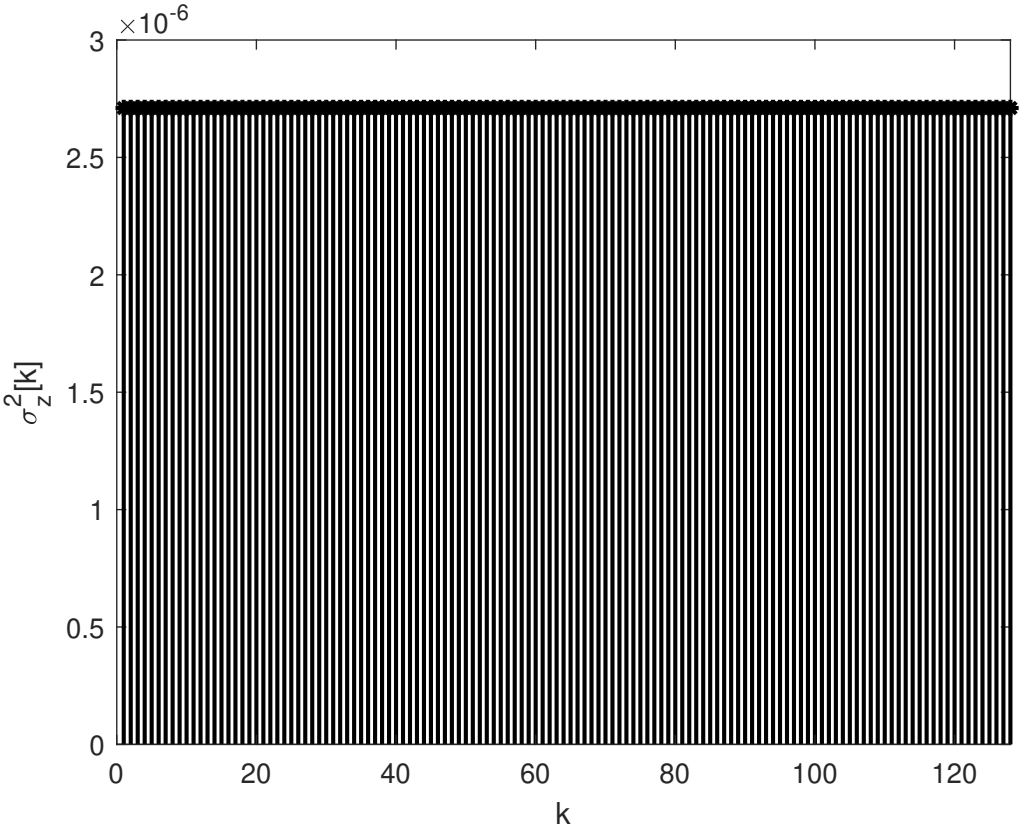

Figure 4.10: Distribution of channel noise variance $\sigma_z^2[k]$ at each data-bearing subcarrier in flat channel (same condition with Figure 4.9
)

The large transmitted power can be allocated uniformly and μ can be selected as 2.5 when $G = 8$ according to Figure 4.7.

Above all, the power allocation of the designed system can be calculated by solving **P2**. With the increasing dimming target, μ can be selected according to the results of the performance. For example, when $\alpha_{dim} = 0.5$, μ can be selected as 2.5 when $G = 4$. More results of the information rate of $G = 4$ and the comparison of C, C_{A}, C_{B} and $\tilde{C}_{\mathrm{B}}$ are presented in Appendix A.

4.3 Summary

Simulation results are shown in Chapter 4 to analyze the performance of the proposed spatial dimming scheme based on SO-OFDM. The performance of the presented SO-OFDM dimming system can be measured by the capacity, signal-to-noise ratio (SNR) of the system. For these cases, the simulation results of the proposed scheme perform well.

Chapter 5

Conclusions and Future Directions

5.1 Conclusion

The thesis proposes a novel water pouring spectrum scheme for spatial dimming based on the SO-OFDM system. The proposed scheme allocates the total power among subcarriers in groups with the optical power constraint and dimming target.

In order to obtain the optimal power allocation, a non-convex problem is formed to maximize the capacity of SO-OFDM with a specified dimming target. This non-convex problem is approximated by a series of convex problems through approximations and constraint relaxation.

The proposed novel power allocation scheme integrates dimming into VLC system based on SO-OFDM. It is observed that more of the power is allocated to subcarriers with low channel noise. This phenomenon suggests that the channel condition plays a vital role in allocating power for each subcarrier. The optimal capacity is close to the capacity with uniform distribution when the dimming target and SNR are high, which agrees well with conventional water filling in the high SNR regime. These

simulation results for the capacity and BER show that the proposed scheme performs well in spatial dimming.

5.2 Future Work

This thesis considers the capacity as a central target to optimize in designing a dimming strategy for spatial optical OFDM systems. As the performance of the proposed scheme has been verified previously, we could also imply this scheme for other directions to obtain a wider range of applications. Some directions could be explored in future work.

First of all, more clipping methods could be discussed in the future. As for clipping noise, symmetric clipping is considered in this thesis. While compared with symmetrical clipping, the asymmetrical clipping in [111] has more extensive applications. Since the problem of asymmetric clipping might be more complicated due to it clips different amounts for both sides of signals, we can consider how to optimize the power allocation scheme with asymmetrical clipping in the future.

What is more, other modulation methods could be considered to combine with dimming methods and obtain better channel capacity. SO-OFDM can reduce PAPR by grouping subcarriers. While other modulation methods can also be considered to obtain greater channel capacity. For example, layered asymmetrically clipped optical orthogonal frequency division multiplexing (LACO-OFDM) in [112] can be used to optimize the power allocation since LACO-OFDM has higher layers and high spectral efficiency which makes it essential to be explored. Additionally, C_{B} is only one of the low bounds of C_{A}. In the future, a tighter low bound of C_{A} will be found to solve the optical problem.

Appendix A

Simulation result with other parameters

A.1 Integration of ${s^*_{g,k}}^{(i)}$

To solve **P2** and **P2-**g, CVX is utilized [107]. Fig. A.1 shows the convergence of ${s^*_{g,k}}^{(i)}$ as the iteration number i increases, in which $\mu = 2.5$, $\alpha_{\text{dim}} = 0.5$ and $G = 8$. In Fig. A.1, $s_{1,1}$, $s_{2,17}$ and $s_{3,33}$ indicate the first nonzero subcarrier in groups 1, 2 and 3 separately. It can be seen that ${s^*_{g,k}}^{(i)}$ converges fast thus that the complexity can be acceptable.

A.2 Iteration of clipping noise

In Section A.2, the iteration of clipping noise with different situations is discussed. The simulation result agrees well with the iteration discussed in Section 4.2.1. **P2** can be solved by iterating clipping noise according to the flow diagram Figure 3.3

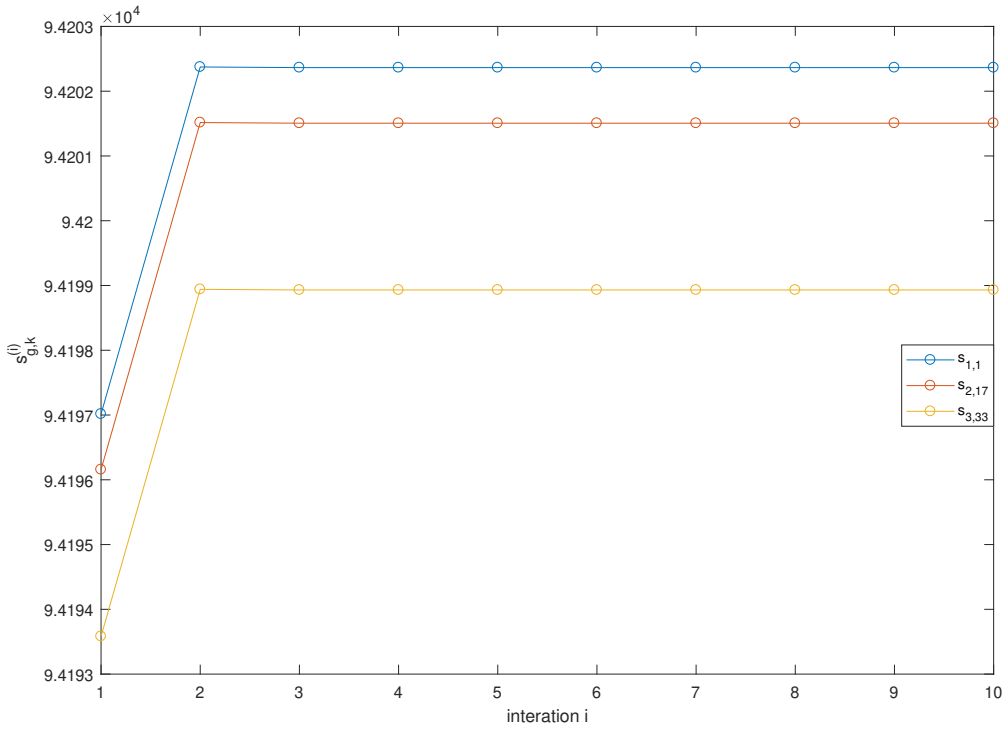

Figure A.1: $s_{\mathrm{g,k}}{}^{(i)}$ vs iteration number i ($\mu = 2.5$, $\alpha_{\mathrm{dim}} = 0.5$ and $G = 8$).

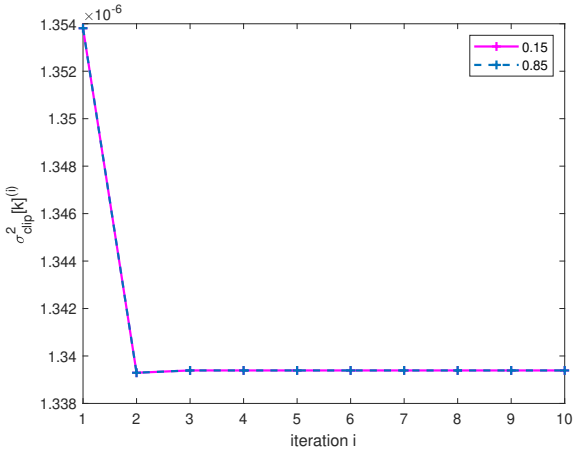

Figure A.2: $\sigma^2_{\text{clip}}[k]^{(i)}$ vs iteration number i ($\mu = 1.5$, $\alpha_{\text{dim}} = 0.15$, $\alpha_{\text{dim}} = 0.85$ and $G = 4$).

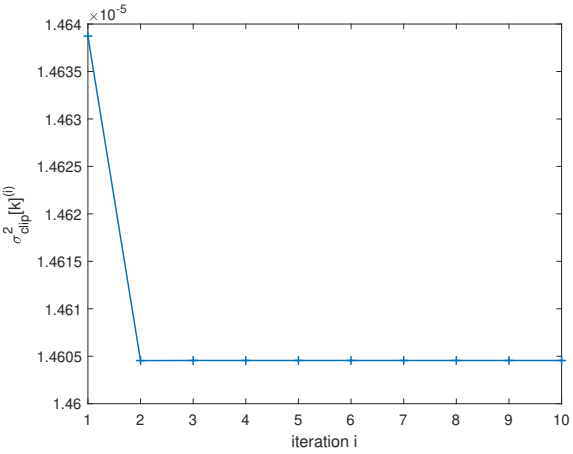

Figure A.3: $\sigma^2_{\text{clip}}[k]^{(i)}$ vs iteration number i ($\mu = 1.5$, $\alpha_{\text{dim}} = 0.5$ and $G = 4$).

in Chapter 3. Figure A.2 to Figure A.3 illustrate the convergence of $\sigma^2_{\text{clip}}[k]^{(i)}$ as iteration number i increases, in which $G = 4$ and $\mu = 1.5$ is fixed for different α_{dim}. It can be seen that the convergence of $\sigma^2_{\text{clip}}[k]^{(i)}$ is quickly in practice in our simulations. As shown in the figure, $\sigma^2_{\text{clip}}[k]^{(i)}$ converges after the second iteration when $G = 4$. The total iteration number i for $\sigma^2_{\text{clip}}[k]^{(i)}$ can be seated as 3 which matches the result discussed in Section 3.2.3.

A.3 Capacity results

A.3.1 Capacity of the system when $G = 4$

For this part, the capacity of the system when $G = 4$ is compared with the power allocation discussed in Section 4.2.3. The following simulation results in this part have selected the case of G=4, α_{dim} and $\mu = 2.5$ for simulation. Results present in this section are similar to the results illustrated in Section 4.2.3 where $G = 8$ is used.

The capacity of equation (3.2.4) discussed in Chapter 3 for $G = 4$ with different dimming levels α_{dim} and different μ is shown in Figure A.4. With the increasing of μ, there is a trade-off between clipping noise variance σ^2_{clip} and useful power σ^2_{useful}. The capacity also increases as the dimming target α_{dim} increases from 0 to 0.5. When α_{dim} keeps increasing from 0.5 to 1, the capacity will decrease due to the reduction of $I_{H,g}$ for LEDs to fit the dynamic range of each LED.

When $\alpha_{\text{dim}} \leq 0.25$ or $\alpha_{\text{dim}} \geq 0.75$, capacity with $\mu = 1.5$ is the largest. This is likely caused by the large clipping noise in these cases. The capacity when $mu = 2.5$ is largest with $0.25 \leq \alpha_{\text{dim}} \leq 0.75$ and reaches the peak when $\alpha_{\text{dim}} = 0.5$ since clipping noise is reduced as μ increases. If mu continues to increase to 3.5 or 4.5 , the capacity will reduce. The findings indicate that the increase of μ causes a reduction in $\sigma^2_{\text{useful}}[k]$ which matches will with these results. When μ is small, e.g., $\mu = 1.5$, the capacity saturates since the clipping noise $\sigma^2_{\text{clip}}[k]$ is much bigger than noise. Furthermore, the capacity is symmetric with respect to $\alpha_{\text{dim}} = 0.5$ and reaches its maximum at $\alpha_{\text{dim}} = 0.5$ as discussed in Section 3.2.

The achievable information rate with uniformly distributed power denoted by dot lines is also shown in Figure A.4 as a reference.

Compared to the rate with uniform power allocation, capacity obtained by solving **P2** is bigger when α_{dim} is small. This is because when α_{dim} is small, SNR is also small and channel noise has a great impact on the power allocation among data-bearing subcarriers. When α_{dim} is large, channel noise is so small compared to signal power that it has a negligible effect on power allocation and in this case uniform distribution among data-carrying subcarriers is close to optimal power allocation.

The details of the channel capacity where α_{dim} is from 0.05 to 0.3 are shown in

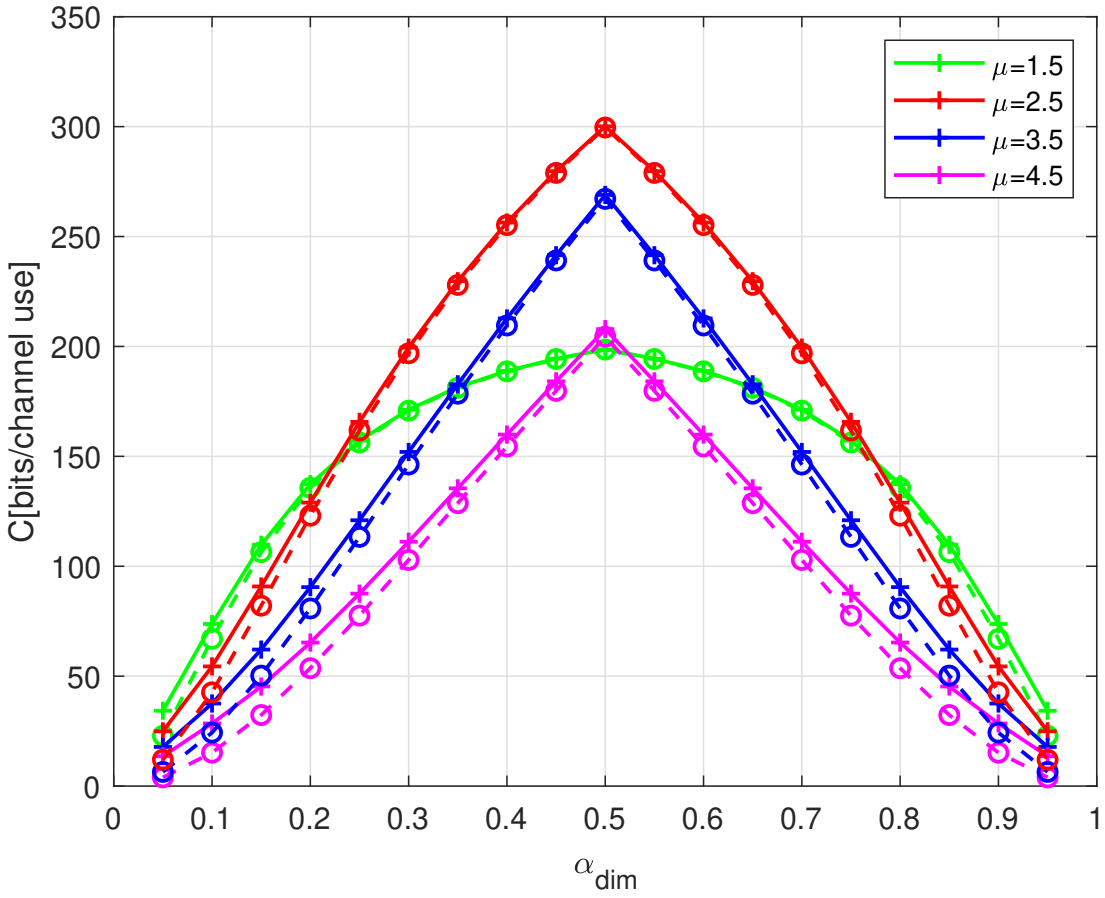

Figure A.4: Capacity of SO-OFDM for different dimming levels with $G = 4$ group (Solid lines show results by solving **P2** and dot lines uniformly distributed $S[k]$).

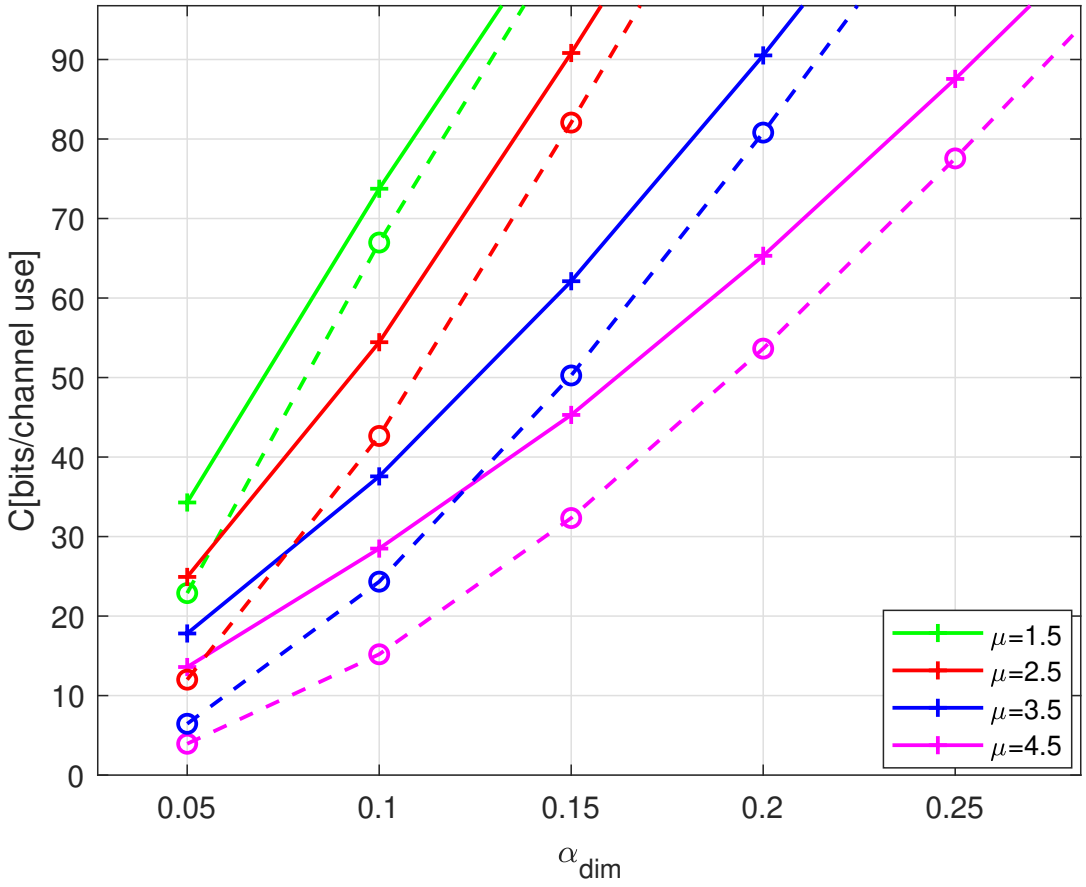

Figure A.5: Zoomed-in-figure for Figure A.4 (Solid lines show results by solving **P2** and dot lines uniformly distributed $S[k]$).

the Figure A.5 which is the zoomed-in-figure of Figure A.4. In Figure A.4, when α_{dim}=0.1, the capacity of the proposed power allocation method is about twice of the capacity for uniform distribution. When α_{dim} is less than 0.5, with the increase of α_{dim}, the gap of channel capacity for the optimal power allocation scheme and the uniform distribution scheme becomes smaller and smaller. This is because when the total power is small, the limited power should be allocated optimally to obtain a larger capacity. However, when the dimming target is large enough, the power is large enough to allocate for each subcarrier, the gap between the optimal power distribution scheme and the uniform power distribution scheme will become smaller and smaller. These phenomena also agree well with conventional water filling in a high SNR regime.

C_{B} , C_{A} and $\tilde{C}_{\text{B}}$ are approximations of the capacity C proposed in Chapter 3 where

$$C=\sum_{g=1}^{G}\sum_{k=(g-1)N_G/2}^{gN_G/2-1}\log_2\left(1+\frac{G_{\text{ele}}^2L_g^2K_g^2s_{g,k}}{\sigma_{\text{z}}^2[k]+\sigma_{\text{clip}}^2[k]}\right). \tag{A.3.1}$$

When μ is large, the clipping noise is very small then even the channel noise will impact BER and the capacity C and be approximated as C_{A} where

$$C_{\text{A}}=\sum_{g=1}^{G}\sum_{k=(g-1)N_G/2}^{gN_G/2-1}\log_2\left(1+\frac{G_{\text{ele}}^2L_g^2K_g^2s_{g,k}}{\sigma_{\text{z}}^2[k]}\right). \tag{A.3.2}$$

C_{B} is less or equal to to C_{A} where

$$C_{\text{B}}=\sum_{g=1}^{G}\log_2\left(1+\frac{G_{\text{ele}}^2L_g^2K_g^2S_g}{\sigma_{\text{z},g}^2}\right). \tag{A.3.3}$$

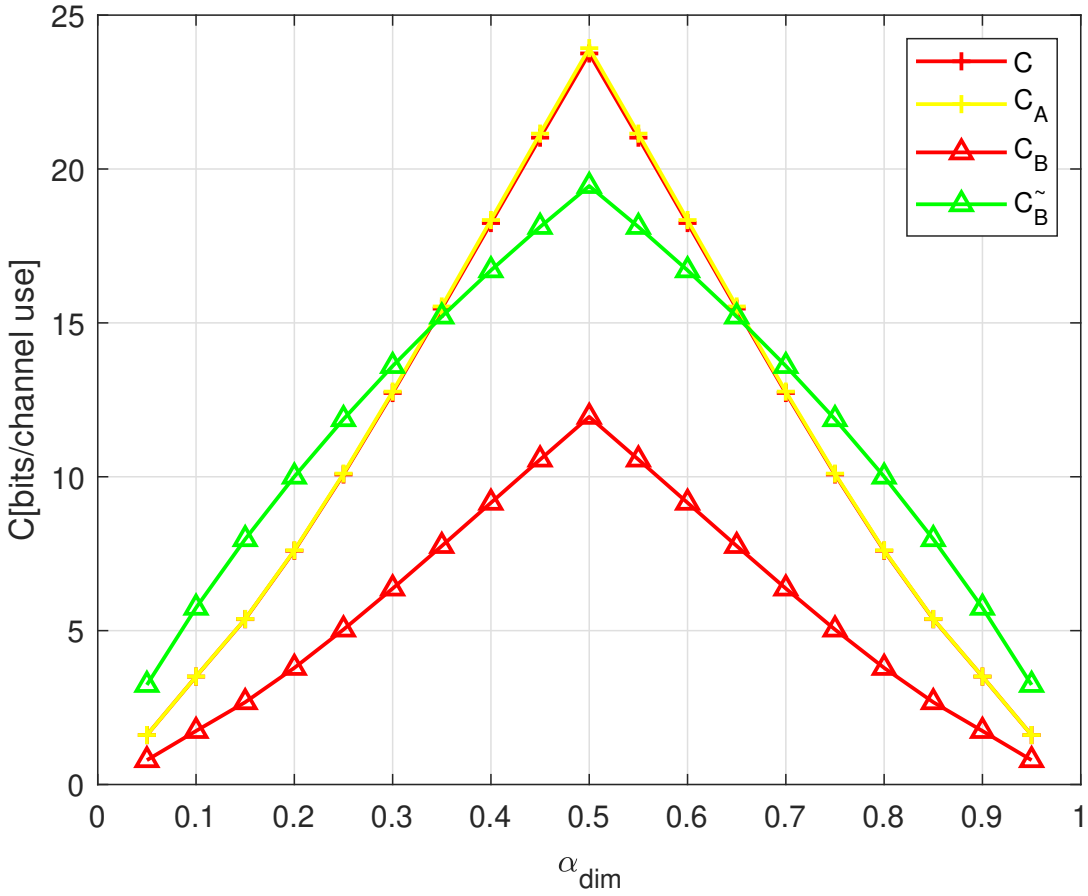

Figure A.6: Different capacity assumption of SO-OFDM for different dimming levels

C_{B} can be approximated as

$$\begin{aligned}\tilde{C}_{\mathrm{B}} &= \sum_{g=1}^{G} \log_2 \left(1 + \frac{\sqrt{N} G_{\mathrm{ele}} L_g K_g}{\sqrt{2}\mu} \frac{I_{\mathrm{H},g}}{\sigma_{\mathrm{z},g}}\right)^2 \\ &= \sum_{g=1}^{G} 2\log_2 \left(1 + \frac{\sqrt{N} G_{\mathrm{ele}} L_g K_g}{\sqrt{2}\mu} \frac{I_{\mathrm{H},g}}{\sigma_{\mathrm{z},g}}\right).\end{aligned} \tag{A.3.4}$$

The simulation result of C , C_{B} , C_{A} and $\tilde{C}_{\mathrm{B}}$ is shown in Figure A.6 with $N = 32$, $\mu = 3.5$ and $G = 8$. As shown in Figure A.6 , $\tilde{C}_{\mathrm{B}}$ is always larger than C_{B}. This

is because compared with C_{B}, some cross terms are add in $\tilde{C}_{\mathrm{B}}$. As shown in Figure A.6, C_{A} is always larger than C_{B} as proved in Theorem 2 in Chapter 3.

Furthermore, a flat channel with noise variance $\sigma_z^2[k]$ is equal at each data-carrying subcarrier shown in Figure A.8, in which $\mu = 2.5$ and $G = 4$. In this condition, the performance of the proposed power allocation scheme and uniform power allocation scheme can be observed in Figure A.7. In Figure A.7, the red solid line represents the channel capacity with the optimal power allocation scheme and the blue dashed line represents the channel capacity with the average power allocation scheme. As shown in the figure, these two lines coincide with each other. This is because the channel is flat, and the noise variance $\sigma_z^2[k]$ corresponding to each subcarrier is the same, so the optimal power allocation scheme is the same as the average power allocation scheme.

A.3.2 BER performance of SO-OFDM dimming

The BER performance of SO-OFDM dimming is illustrate against SNR and different dimming levels α_{dim} with $\mu = 2.5$ and $G = 4$ in Figure A.9. In the numerical result for the simulation, SNR is considered as SNDR which is defined in (3.1.19). For the given α_{dim}, $\sigma^2_{\mathrm{useful}}[k]$ and the noise power can be calculate according to (3.1.10) and (3.1.11). The relationship between BER and SNDR can be written as

$$\begin{aligned}\mathrm{BER}[k] =& \frac{4(\sqrt{M}-1)}{\sqrt{M\log_2(M)}} Q\left(\sqrt{\frac{3\log_2(M)}{M-1}(\mathrm{SNDR}[k])}\right) \\ &+ \frac{4(\sqrt{M}-2)}{\sqrt{M\log_2(M)}} Q\left(3\sqrt{\frac{3\log_2(M)}{M-1}(\mathrm{SNDR}[k])}\right).\end{aligned} \tag{A.3.5}$$

according to (3.1.20). In Figure A.9, when the value of SNR is small, such as when SNR is less than 5dB, AWGN $\sigma_{\mathrm{z}}^2[k]$ is the dominant source of the noise in $\sigma_{\mathrm{z}}^2[k]+\sigma_{\mathrm{clip}}^2[k]$

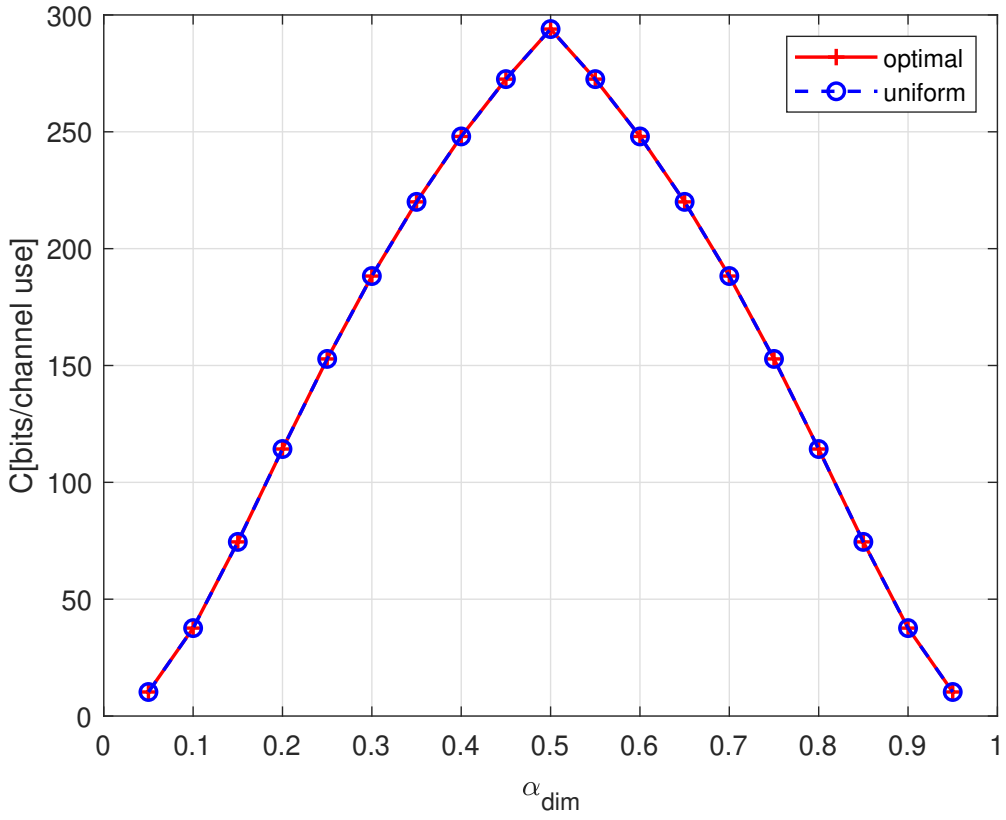

Figure A.7: Capacity of SO-OFDM for different dimming levels with $G = 4$ groups in flat channel (Solid lines show results by solving **P2** and dot lines uniformly distributed $S[k]$).

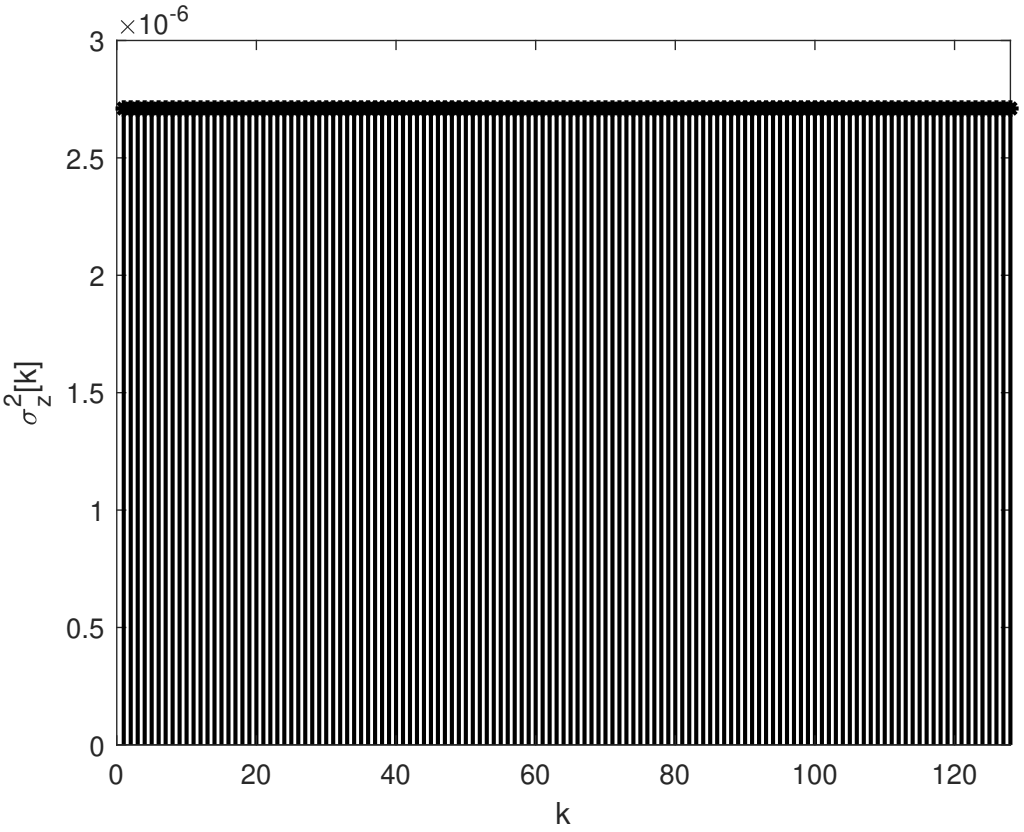

Figure A.8: Distribution of noise variance $\sigma_z^2[k]$ at each data-bearing subcarrier in flat channel (same condition with Figure A.7)

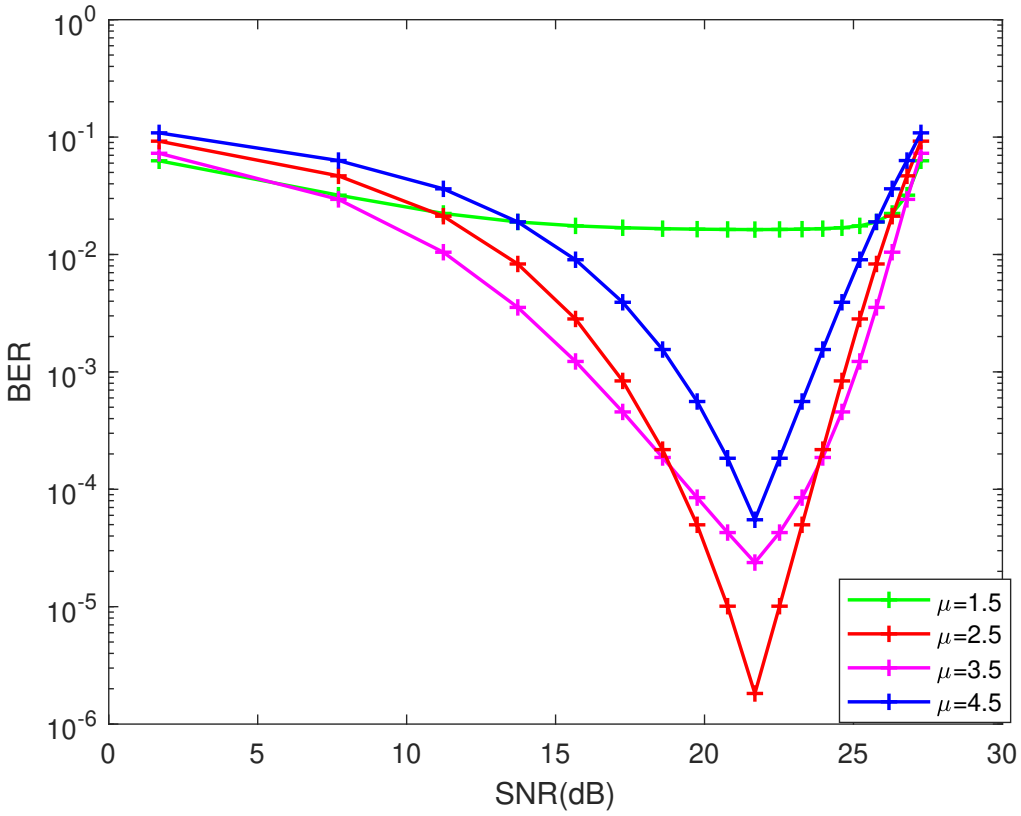

Figure A.9: BER performance of SO-OFDM with the increasing of SNR and $G = 4$ group

[4]. Since AWGN is equal with different μ, the value of BER will be mainly influenced by the useful subcarrier power. As discussed previously, the increasing of μ will decrease the useful subcarrier power which leads to the result in Figure A.9 when SNR is small. Then, with the increase of SNR, clipping noise dominates the source of noise which causes the poor performance of BER for $\mu = 1.5$. While there is a trade-off between the increasing of the clipping distortion and useful subcarrier power for different values of μ. Therefore, when the value of SNR is approximately 24 dB, the pink line for $\mu = 2.5$ and the green line for $\mu = 3.5$ intersect.

Appendix B

Proof of equations proposed in Chapter 3

This appendix presents the equation proposed in Chapter 3.

B.1 Proof of (3.1.18) in Chapter 3

Based on (3.1.3) in Chapter 3,

$$\begin{aligned} &\mathrm{E}\left\{c_g[n]\right\}^2 = \mathrm{E}\left\{u_g^2[n]\right\} - K_{\mathrm{g}}^2\sigma_g^2 \\ &= \sigma_g^2\Big(\operatorname{erf}(\gamma_g) - \operatorname{erf}^2(\gamma_g) + 4\gamma_g^2(1-\operatorname{erf}(\gamma_g)) - \frac{2\gamma_g}{\sqrt{\pi}}\exp\left(-\gamma_g^2\right)\Big). \end{aligned} \tag{B.1.1}$$

Substituting (3.1.16) and (B.1.10) into (3.1.15) leads to Theo. 1, where

$$\mathrm{E}\left\{u_g^2[n]\right\} = \sigma_g^2 \operatorname{erf}\left(\frac{c}{\sqrt{2}\sigma_g}\right) + c^2 \operatorname{erfc}\left(\frac{c}{\sqrt{2}\sigma_g}\right) - \frac{2\sigma_g c}{\sqrt{2\pi}}\exp\left(-\frac{c^2}{2\sigma_g^2}\right). \tag{B.1.2}$$

The proof of equation B.1.2 is as follows.

Proof.

$$\mathrm{E}\left\{u_g[n]x_g[n]\right\} = \mathrm{E}\left\{K_g x_g x_g[n]\right\} \quad = K_g \mathrm{E}\left\{x_g^2[n]\right\} = K_g \sigma_g^2 \tag{B.1.3}$$

where according to Bussgang's theorem we have

$$K_g = \frac{\mathrm{E}\left\{u_g[n]x_g[n]\right\}}{\sigma_g^2} = \left(1 - \mathrm{erfc}\left(\frac{I_{\mathrm{H}}}{\sqrt{2}\sigma_g}\right)\right) \tag{B.1.4}$$

$$\begin{aligned}
\mathrm{E}\left\{\mathrm{c_g^2[n]}\right\} &= \mathrm{E}\left\{\left(u_g[n] - K_g x_g[n]\right) c_g[n]\right\} = \mathrm{E}\left\{u_g[n]c_g[n]\right\} - 0 \\
&= \mathrm{E}\left\{u_g[n]\left(u_g[n] - K_g x_g[n]\right)\right\} \\
&= \mathrm{E}\left\{u_g^2[n]\right\} - K_g \mathrm{E}\left\{u_g[n]x_g[n]\right\} \\
&= \mathrm{u_g^2[n]} - K_g^2 \sigma_g^2
\end{aligned} \tag{B.1.5}$$

Below is acquiring $\mathrm{u_g^2[n]}$.

$$\begin{aligned}
\mathrm{E}\left\{u_g^2[n]\right\} &= \int_{-\infty}^{\infty} u_g^2 \times f(u_g) du_g \\
&= \int_{-\infty}^{0} u_g^2 \times f(u_g) du_g + \int_{0}^{\infty} u_g^2 \times f(u_g) du_g \\
&= \int_{-\infty}^{I_L} u_g^2 \times f(u_g) du_g + \int_{I_L}^{0} u_g^2 \times f(u_g) du_g + \int_{0}^{I_H} u_g^2 \times f(u_g) du_g \\
&+ \int_{I_H}^{\infty} u_g^2 \times f(u_g) du_g
\end{aligned} \tag{B.1.6}$$

For symmetric clipping, $I_{\mathrm{L}} = -I_{\mathrm{H}}$, so

$$\begin{aligned} \mathrm{E}\left\{u_g^2[n]\right\} = &\int_{-\infty}^{I_{\mathrm{L}}} u_g^2 \times f(u_g)\mathrm{d}u_g + 2\int_{0}^{I_{\mathrm{H}}} u_g^2 \times f(u_g)\mathrm{d}u_g \\ &+ \int_{I_{\mathrm{H}}}^{\infty} u_g^2 \times f(u_g)\mathrm{d}u_g \end{aligned} \tag{B.1.7}$$

$$\begin{aligned} \mathrm{E}\left\{u_g^2[n]\right\} &= \int_{-\infty}^{I_{\mathrm{L}}} {I_{\mathrm{H}}}^2 \times f(u_g)\mathrm{d}u_g + 2\int_{0}^{I_{\mathrm{H}}} u_g^2 \times f(u_g)\mathrm{d}u_g + \int_{I_{\mathrm{H}}}^{\infty} {I_{\mathrm{H}}}^2 \times f(u_g)\mathrm{d}u_g \\ &= \sigma_g^2 \,\mathrm{erf}\left(\frac{I_{\mathrm{H}}}{\sqrt{2}\sigma_g}\right) + I_{\mathrm{H}}^2 \,\mathrm{erfc}\left(\frac{I_{\mathrm{H}}}{\sqrt{2}\sigma_g}\right) - \frac{2\sigma_g I_{\mathrm{H}}}{\sqrt{2\pi}} \exp\left(-\frac{I_{\mathrm{H}}^2}{2\sigma_g^2}\right) \end{aligned} \tag{B.1.8}$$

where erf(z) means error function, defined as:

$$\mathrm{erf}(z) = \frac{2}{\sqrt{\pi}} \int_0^z e^{-t^2} dt \tag{B.1.9}$$

Therefore, we have

$$\begin{aligned} &\mathrm{E}\left\{c_g[n]\right\}^2 = \mathrm{E}\left\{u_g^2[n]\right\} - K_{\mathrm{g}}^2 \sigma_g^2 \\ &= \sigma_g^2 \Big(\mathrm{erf}\left(\gamma_g\right) - \mathrm{erf}^2\left(\gamma_g\right) + 4\gamma_g^2(1 - \mathrm{erf}\left(\gamma_g\right)) - \frac{2\gamma_g}{\sqrt{\pi}} \exp\left(-\gamma_g^2\right) \Big). \end{aligned} \tag{B.1.10}$$

□

B.2 Proof of (3.2.9)in Chapter 3

$$\sum_{k=(g-1)N_G/2}^{gN_G/2-1} \frac{s_{g,k}}{\sigma_{\mathrm{z}}^2[k]} \geq \frac{\sum_{k=(g-1)N_G/2}^{gN_G/2-1} s_{g,k}}{\sum_{k=(g-1)N_G/2}^{gN_G/2-1} \sigma_{\mathrm{z}}^2[k]}. \tag{B.2.1}$$

Proof. For the first term of (B.2.6)

$$\frac{s_{1,1}}{\sigma_{\mathrm{z}}^2[1]} \geq \frac{s_{1,1}}{\sigma_{\mathrm{z}}^2[1]}. \tag{B.2.2}$$

For the first two terms of (3.2.9)

$$\begin{aligned} \frac{s_{1,1}}{\sigma_{\mathrm{z}}^2[1]} + \frac{s_{1,2}}{\sigma_{\mathrm{z}}^2[2]} - \frac{s_{1,1}+s_{1,2}}{\sigma_{\mathrm{z}}^2[1]+\sigma_{\mathrm{z}}^2[2]} &= \frac{s_{1,1}\sigma_{\mathrm{z}}^2[2] + s_{1,2}\sigma_{\mathrm{z}}^2[1]}{\sigma_{\mathrm{z}}^2[1]\sigma_{\mathrm{z}}^2[2]} - \frac{s_{1,1}+s_{1,2}}{\sigma_{\mathrm{z}}^2[1]+\sigma_{\mathrm{z}}^2[2]} \\ &= \frac{s_{1,1}\sigma_{\mathrm{z}}^4[2] + s_{1,2}\sigma_{\mathrm{z}}^4[1]}{(\sigma_{\mathrm{z}}^2[1]+\sigma_{\mathrm{z}}^2[2])\sigma_{\mathrm{z}}^2[1]\sigma_{\mathrm{z}}^2[2]} \geq 0. \end{aligned} \tag{B.2.3}$$

So,

$$\frac{s_{1,1}}{\sigma_{\mathrm{z}}^2[1]} + \frac{s_{1,2}}{\sigma_{\mathrm{z}}^2[2]} \geq \frac{s_{1,1}+s_{1,2}}{\sigma_{\mathrm{z}}^2[1]+\sigma_{\mathrm{z}}^2[2]} \tag{B.2.4}$$

For the k-th term, assuming previous $k-1$ term equal to S and σ_{sum}, so

$$\frac{s_{g,k}}{\sigma_{\mathrm{z}}^2[k]} + \frac{S}{\sigma_{sum}} \geq \frac{s_{g,k}+S}{\sigma_{\mathrm{z}}^2[k]+\sigma_{sum}} \tag{B.2.5}$$

According to mathematical induction

$$\sum_{k=(g-1)N_G/2}^{gN_G/2-1} \frac{s_{g,k}}{\sigma_{\mathrm{z}}^2[k]} \geq \frac{\sum_{k=(g-1)N_G/2}^{gN_G/2-1} s_{g,k}}{\sum_{k=(g-1)N_G/2}^{gN_G/2-1} \sigma_{\mathrm{z}}^2[k]}. \tag{B.2.6}$$

□

Bibliography

[1] H. Haas, "LiFi is a paradigm-shifting 5G technology," *Reviews in Physics*, vol. 3, pp. 26–31, 2018.

[2] M. S. A. Mossaad, S. Hranilovic, and L. Lampe, "Visible Light Communications Using OFDM and Multiple LEDs," *IEEE Transactions on Communications*, vol. 63, no. 11, pp. 4304–4313, Nov 2015.

[3] H. Elgala, R. Mesleh, and H. Haas, "Predistortion in optical wireless transmission using OFDM," in *2009 Ninth International Conference on Hybrid Intelligent Systems*, vol. 2. IEEE, 2009, pp. 184–189.

[4] F. Zafar, D. Karunatilaka, and R. Parthiban, "Dimming schemes for visible light communication: the state of research," *Wireless Communications IEEE*, vol. 22, no. 2, pp. 29–35, 2015.

[5] F. R. Gfeller and U. Bapst, "Wireless in-house data communication via diffuse infrared radiation," *Proceedings of the IEEE*, vol. 67, no. 11, pp. 1474–1486, 1979.

[6] A. Z. Suriza, S. Akter, and M. Shahnan, in *2017 IEEE 4th International Conference on Smart Instrumentation, Measurement and Application (ICSIMA).*

[7] R. Mesleh, H. Elgala, and H. Haas, "LED nonlinearity mitigation techniques in optical wireless OFDM communication systems," *Journal of Optical Communications and Networking*, vol. 4, no. 11, pp. 865–875, 2012.

[8] M. S. Mossaad and S. Hranilovic, "Practical OFDM signalling for visible light communications using spatial summation," in *2014 27th Biennial Symposium on Communications (QBSC)*. IEEE, 2014, pp. 5–9.

[9] Y. Yang, Z. Zeng, J. Cheng, and C. Guo, "An enhanced DCO-OFDM scheme for dimming control in visible light communication systems," *IEEE Photonics Journal*, vol. 8, no. 3, pp. 1–13, 2016.

[10] G. M. D. T. Forecast, "Cisco Visual Networking Index: Global Mobile Data Traffic Forecast Update, 2017–2022," *Update*, vol. 2017, p. 2022, 2019.

[11] H. Zhang, N. Liu, K. Long, J. Cheng, V. C. M. Leung, and L. Hanzo, "Energy Efficient Subchannel and Power Allocation for Software-defined Heterogeneous VLC and RF Networks," *IEEE Journal on Selected Areas in Communications*, vol. 36, no. 3, pp. 658–670, March 2018.

[12] S. Wu, H. Wang, and C. Youn, "Visible light communications for 5G wireless networking systems: from fixed to mobile communications," *IEEE Network*, vol. 28, no. 6, pp. 41–45, 2014.

[13] T. Wang, F. Yang, L. Cheng, and J. Song, "Spectral-efficient generalized spatial modulation based hybrid dimming scheme with LACO-OFDM in VLC," *IEEE Access*, vol. 6, pp. 41 153–41 162, 2018.

[14] J. Lian, Z. Vatansever, M. Noshad, and M. Brandt-Pearce, "Indoor visible light communications, networking, and applications," *Journal of Physics: Photonics*, vol. 1, no. 1, p. 012001, 2019.

[15] C. Medina, M. Zambrano, and K. Navarro, "Led based visible light communication: Technology, applications and challenges-a survey," *International Journal of Advances in Engineering & Technology*, vol. 8, no. 4, p. 482, 2015.

[16] N. Chi, H. Haas, M. Kavehrad, T. D. Little, and X.-L. Huang, "Visible light communications: demand factors, benefits and opportunities [Guest Editorial]," *IEEE Wireless Communications*, vol. 22, no. 2, pp. 5–7, 2015.

[17] Q. Wang, Z. Wang, and L. Dai, "Multiuser MIMO-OFDM for visible light communications," *IEEE Photonics Journal*, vol. 7, no. 6, pp. 1–11, 2015.

[18] A. Yariv, "Internal modulation in multimode laser oscillators," *Journal of Applied Physics*, vol. 36, no. 2, pp. 388–391, 1965.

[19] Z. J. W. E. L. Qiang, "New test method for PI curve of LD/LED [J]," *Electronic Measurement Technology*, vol. 8, 2012.

[20] A. G. Bell, W. Adams, W. Preece *et al.*, "Discussion on" The photophone and the conversion of radiant energy into sound"," *Journal of the Society of Telegraph Engineers*, vol. 9, no. 34, pp. 375–383, 1880.

[21] Y. Tanaka, S. Haruyama, and M. Nakagawa, "Wireless optical transmissions with white colored LED for wireless home links," in *11th IEEE International Symposium on Personal Indoor and Mobile Radio Communications. PIMRC 2000. Proceedings (Cat. No. 00TH8525)*, vol. 2. IEEE, 2000, pp. 1325–1329.

[22] T. Komine and M. Nakagawa, "Fundamental analysis for visible-light communication system using LED lights," *IEEE transactions on Consumer Electronics*, vol. 50, no. 1, pp. 100–107, 2004.

[23] K. Ying, H. Qian, R. J. Baxley, and G. T. Zhou, "MIMO transceiver design in dynamic-range-limited VLC systems," *IEEE Photonics Technology Letters*, vol. 28, no. 22, pp. 2593–2596, 2016.

[24] J. Gancarz, H. Elgala, and T. D. Little, "Impact of lighting requirements on VLC systems," *IEEE Communications Magazine*, vol. 51, no. 12, pp. 34–41, 2013.

[25] M. B. Rahaim and T. D. Little, "Toward practical integration of dual-use VLC within 5G networks," *IEEE Wireless Communications*, vol. 22, no. 4, pp. 97–103, 2015.

[26] J. M. Kahn and J. R. Barry, "Wireless infrared communications," *Proceedings of the IEEE*, vol. 85, no. 2, pp. 265–298, 1997.

[27] L. U. Khan, "Visible light communication: Applications, architecture, standardization and research challenges," *Digital Communications and Networks*, vol. 3, no. 2, pp. 78–88, 2017.

[28] A. Astrin, "IEEE Standard for Local and metropolitan area networks part 15.6: Wireless Body Area Networks," *IE EE Std 802.15. 6*, 2012.

[29] S. Rajagopal, R. D. Roberts, and S.-K. Lim, "IEEE 802.15. 7 visible light communication: modulation schemes and dimming support," *IEEE Communications Magazine*, vol. 50, no. 3, pp. 72–82, 2012.

[30] J.-P. Javaudin, M. Bellec, D. Varoutas, and V. Suraci, "OMEGA ICT project: Towards convergent Gigabit home networks," in *2008 IEEE 19th International Symposium on Personal, Indoor and Mobile Radio Communications*. IEEE, 2008, pp. 1–5.

[31] M. Uysal, O. Narmanlioglu, T. Baykas, and R. Kizilirmak, "Adaptive MIMO OFDM PHY Proposal for IEEE 802.15. 7r1," *doc: IEEE*, vol. 802, pp. 15–16, 2016.

[32] V. Jungnickel, M. Uysal, N. Serafimovski, T. Baykas, D. O'Brien, E. Ciaramella, Z. Ghassemlooy, R. Green, H. Haas, P. A. Haigh *et al.*, "A European view on the next generation optical wireless communication standard," in *2015 IEEE Conference on Standards for Communications and Networking (CSCN)*. IEEE, 2015, pp. 106–111.

[33] J. Luna-Rivera, R. Perez-Jimenez, J. Rabadan-Borjes, J. Rufo-Torres, V. Guerra, and C. Suarez-Rodriguez, "Multiuser CSK scheme for indoor visible light communications," *Optics express*, vol. 22, no. 20, pp. 24 256–24 267, 2014.

[34] A. A. Purwita and H. Haas, "Studies of Flatness of LiFi Channel for IEEE 802.11bb," in *2020 IEEE Wireless Communications and Networking Conference (WCNC)*, 2020, pp. 1–6.

[35] M. Uysal, F. Miramirkhani, T. Baykas, and K. Qaraqe, "Ieee 802.11 bb reference channel models for indoor environments," Tech. Rep., 2018.

[36] H. Elgala and T. D. Little, "Reverse polarity optical-OFDM (RPO-OFDM): dimming compatible OFDM for gigabit VLC links," *Optics express*, vol. 21, no. 20, pp. 24 288–24 299, 2013.

[37] Y. Suh, C.-H. Ahn, and J. K. Kwon, "Dual-codeword allocation scheme for dimmable visible light communications," *IEEE Photonics Technology Letters*, vol. 25, no. 13, pp. 1274–1277, 2013.

[38] S. Lee, B.-G. Ahn, M. Ju, and Y. Park, "A modified VPPM algorithm of VLC systems suitable for fast dimming environment," *Optics Communications*, vol. 365, pp. 43–48, 2016.

[39] X. You, J. Chen, H. Zheng, and C. Yu, "Efficient data transmission using MPPM dimming control in indoor visible light communication," *IEEE Photonics Journal*, vol. 7, no. 4, pp. 1–12, 2015.

[40] N. Chi, *LED-based visible light Communications*. Springer, 2018.

[41] L. Feng, R. Q. Hu, J. Wang, P. Xu, and Y. Qian, "Applying VLC in 5G Networks: Architectures and Key Technologies," *IEEE Network*, vol. 30, no. 6, pp. 77–83, 2016.

[42] T. Komine and M. Nakagawa, "Fundamental analysis for visible-light communication system using LED lights, year=2004, volume=50, number=1, pages=100-107, doi=10.1109/TCE.2004.1277847," *IEEE Transactions on Consumer Electronics*.

[43] N. Chi and J. Shi, "Investigation on overlapping interference on vlc networks consisting of multiple leds," *ICT Express*, vol. 1, no. 2, pp. 63 – 66,

2015. [Online]. Available: http://www.sciencedirect.com/science/article/pii/S2405959515000053

[44] A. Costanzo, V. Loscrí, V. Deniau, and J. Rioult, "On the Interference Immunity of Visible Light Communication (VLC)," in *IEEE Global Communications Conference (GLOBECOM 2020)*, 2020.

[45] A. U. Guler, T. Braud, and P. Hui, "Spatial Interference Detection for Mobile Visible Light Communication," in *2018 IEEE International Conference on Pervasive Computing and Communications (PerCom)*. IEEE, 2018, pp. 1–10.

[46] P. L. L. Company., "Philips Lighting," [EB/OL], https://www.signify.com/global/innovation/trulifi Accessed 30 November, 2020.

[47] A. Funahashi, K. Kobayashi, H. Okada, and M. Katayama, "i-LightHouse: A Visible Light Communication system for the visually impaired," in *IEEE International Symposium on Personal Indoor Mobile Radio Communications*, 2012.

[48] V. Company, "Light Communication (LiFi) for FTTx Solutions – Enabling last-mile broadband connectivity," [EB/OL], https://www.velmenni.com/blog/LiFi-for-fttx-solutions/ Accessed 17 December, 2020.

[49] A. Tsiatmas, C. P. Baggen, F. M. Willems, J.-P. M. Linnartz, and J. W. Bergmans, "An illumination perspective on visible light communications," *IEEE Communications Magazine*, vol. 52, no. 7, pp. 64–71, 2014.

[50] M. Miki, S. Fujimoto, Y. Motoya, and R. Okunishi, "Maximization of the Average Color Rendering Index of Color Temperature and Illuminance Constraints,"

in *2013 IEEE International Conference on Systems, Man, and Cybernetics*. IEEE, 2013, pp. 4583–4588.

[51] Y. Yang, Z. Zeng, J. Cheng, and C. Guo, "A novel hybrid dimming control scheme for visible light communications," *IEEE Photonics Journal*, vol. 9, no. 6, pp. 1–12, 2017.

[52] J. Gancarz, H. Elgala, and T. D. C. Little, "Impact of lighting requirements on VLC systems," *IEEE Communications Magazine*, vol. 51, no. 12, pp. 34–41, December 2013.

[53] "IEEE Recommended Practices for Modulating Current in High-Brightness LEDs for Mitigating Health Risks to Viewers," 2015.

[54] Y. M. Cho, S. H. Ryu, B. R. Lee, K. H. Kim, E. Lee, and J. Choi, "Effects of artificial light at night on human health: A literature review of observational and experimental studies applied to exposure assessment," *Chronobiology International*, pp. 1294–1310, 2015.

[55] H. G. Sandalidis, A. Vavoulas, T. A. Tsiftsis, and N. Vaiopoulos, "Illumination, data transmission, and energy harvesting: the threefold advantage of VLC," *Applied optics*, vol. 56, no. 12, pp. 3421–3427, 2017.

[56] A. Žukauskas and M. S. Shur, *Color Rendering Metrics: Status, Methods, and Future Development*. Springer International Publishing, 2017.

[57] Wu, Chung, Y., Guo, Chang, Z., Xu, J., and M., "Microwave-assisted high-speed modulation of semiconductor lasers," *Can.j.phys*, 1992.

[58] A. Pradana, N. Ahmadi, and T. Adionos, "Design and implementation of visible light communication system using pulse width modulation," in *2015 International Conference on Electrical Engineering and Informatics (ICEEI)*. IEEE, 2015, pp. 25–30.

[59] J. De Clercq and R. Thielemans, "Led lighting that has continuous and adjustable color temperature (ct), while maintaining a high cri," Jan. 7 2010, uS Patent App. 12/518,860.

[60] H. Elgala, R. Mesleh, and H. Haas, "Indoor broadcasting via white LEDs and OFDM," *IEEE Transactions on consumer electronics*, vol. 55, no. 3, pp. 1127–1134, 2009.

[61] S. H. Lee, S.-Y. Jung, and J. K. Kwon, "Modulation and coding for dimmable visible light communication," *IEEE Communications Magazine*, vol. 53, no. 2, pp. 136–143, 2015.

[62] A. R. Bahai, B. R. Saltzberg, and M. Ergen, *Multi-carrier digital communications: theory and applications of OFDM*. Springer Science & Business Media, 2004.

[63] S.-H. Yang, E.-M. Jeong, D.-R. Kim, H.-S. Kim, Y.-H. Son, and S.-K. Han, "Indoor three-dimensional location estimation based on LED visible light communication," *Electronics Letters*, vol. 49, no. 1, pp. 54–56, 2013.

[64] A. A. Al-jzari, I. Kostanic, and K. H. M. Mabrok, "Effect of variable cyclic prefix length on OFDM system performance over different wireless channel models," *Univers. J. Commun. Networ*, vol. 3, no. 1, pp. 7–14, 2015.

[65] J. Dang, M. Wu, L. Wu, and Z. Zhang, "Transceiver Design for MIMO DCO-OFDM in Visible Light Communication," in *Visible Light Communications*. IntechOpen, 2017.

[66] I. Stefan, H. Elgala, and H. Haas, "Study of dimming and LED nonlinearity for ACO-OFDM based VLC systems," 2012.

[67] J. Armstrong and A. J. Lowery, "Power efficient optical OFDM," *Electronics letters*, vol. 42, no. 6, pp. 370–372, 2006.

[68] D. Tsonev, S. Sinanovic, and H. Haas, "Novel unipolar orthogonal frequency division multiplexing (U-OFDM) for optical wireless," in *2012 IEEE 75th Vehicular Technology Conference (VTC Spring)*. IEEE, 2012, pp. 1–5.

[69] Q. Wang, Z. Wang, and L. Dai, "Asymmetrical hybrid optical OFDM for visible light communications with dimming control," *IEEE Photonics Technology Letters*, vol. 27, no. 9, pp. 974–977, 2015.

[70] Q. Wang, C. Qian, X. Guo, Z. Wang, D. G. Cunningham, and I. H. White, "Layered ACO-OFDM for intensity-modulated direct-detection optical wireless transmission," *Optics Express*, vol. 23, no. 9, pp. 12 382–12 393, 2015.

[71] H. Elgala and T. D. Little, "SEE-OFDM: Spectral and energy efficient OFDM for optical IM/DD systems," in *2014 IEEE 25th annual international symposium on personal, indoor, and mobile radio communication (PIMRC)*. IEEE, 2014, pp. 851–855.

[72] ——, "Polar-based OFDM and SC-FDE links toward energy-efficient Gbps transmission under IM-DD optical system constraints," *IEEE/OSA Journal of Optical Communications and Networking*, vol. 7, no. 2, pp. A277–A284, 2015.

[73] ——, "P-OFDM: spectrally efficient unipolar OFDM," in *OFC 2014*. IEEE, 2014, pp. 1–3.

[74] J. Wang, Y. Xu, X. Ling, R. Zhang, Z. Ding, and C. Zhao, "PAPR analysis for OFDM visible light communication," *Optics express*, vol. 24, no. 24, pp. 27 457–27 474, 2016.

[75] H. Sugiyama, S. Haruyama, and M. Nakagawa, "Brightness Control Methods for Illumination and Visible-Light Communication Systems, year=2007, volume=, number=, pages=78-78, doi=10.1109/ICWMC.2007.26," in *2007 Third International Conference on Wireless and Mobile Communications (ICWMC'07)*.

[76] X. Huang, X. Fu, and W. Xu, "Incremental scheduling scheme for indoor visible light communication," *Electronics Letters*, vol. 51, no. 3, pp. 268–270, 2015.

[77] O. Babatundi, L. Qian, and J. Cheng, "Downlink scheduling in visible light communications," in *2014 Sixth International Conference on Wireless Communications and Signal Processing (WCSP)*. IEEE, 2014, pp. 1–6.

[78] J. Rogers *et al.*, "Algorithm for color corrected analog dimming in multi-color LED system," Apr. 29 2014, uS Patent 8,710,768.

[79] Y. Hu and M. M. Jovanovic, "LED driver with self-adaptive drive voltage," *IEEE Transactions on Power Electronics*, vol. 23, no. 6, pp. 3116–3125, 2008.

[80] X. Xu and X. Wu, "High dimming ratio LED driver with fast transient boost converter," in *2008 IEEE Power Electronics Specialists Conference*. IEEE, 2008, pp. 4192–4195.

[81] G. Pathak, A. R. Saxena, and P. Bansal, "Review of dimming techniques for solid-state LED lights," *International Journal of Advanced Engineering Research and Technology (IJAERT)*, vol. 2, no. 4, pp. 108–114, 2014.

[82] R. Lenk and C. Lenk, *Practical lighting design with LEDs*. John Wiley & Sons, 2017.

[83] E. Cheung, "High voltage boost/led controller provides 3000: 1 pwm dimming ratio," *Linear Technology application note*, 2006.

[84] M. Dyble, N. Narendran, A. Bierman, and T. Klein, "Impact of dimming white LEDs: Chromaticity shifts due to different dimming methods," in *Fifth international conference on solid state lighting*, vol. 5941. International Society for Optics and Photonics, 2005, p. 59411H.

[85] "An effective LED dimming approach, author=Narra, Prathyusha and Zinger, Donald S," in *Conference Record of the 2004 IEEE Industry Applications Conference, 2004. 39th IAS Annual Meeting.*, vol. 3. IEEE, 2004, pp. 1671–1676.

[86] D. Kelly, "Visual contrast sensitivity," *Optica Acta: International Journal of Optics*, vol. 24, no. 2, pp. 107–129, 1977.

[87] D. Gacio, J. M. Alonso, J. Garcia, L. Campa, M. J. Crespo, and M. Rico-Secades, "PWM series dimming for slow-dynamics HPF LED drivers: The

high-frequency approach," *IEEE Transactions on Industrial Electronics*, vol. 59, no. 4, pp. 1717–1727, 2011.

[88] H. Sugiyama, S. Haruyama, and M. Nakagawa, "Brightness control methods for illumination and visible-light communication systems," in *2007 Third International Conference on Wireless and Mobile Communications (ICWMC'07)*. IEEE, 2007, pp. 78–78.

[89] L. Svilainis, "Comparison of the EMI performance of LED PWM dimming techniques for LED video display application," *Journal of Display Technology*, vol. 8, no. 3, pp. 162–165, 2012.

[90] Z. Wang, C. Guo, Y. Yang, and Q. Li, "A novel dimming scheme for indoor MIMO visible light communication based on antenna selection," in *2016 IEEE 83rd Vehicular Technology Conference (VTC Spring)*. IEEE, 2016, pp. 1–5.

[91] Y. Yang, Z. Zeng, J. Cheng, and C. Guo, "Spatial dimming scheme for optical OFDM based visible light communication," *Optics express*, vol. 24, no. 26, pp. 30 254–30 263, 2016.

[92] A. Z. Suriza, S. Akter, and M. Shahnan, "Preliminary analysis of dimming property for visible light communication," in *2017 IEEE 4th International Conference on Smart Instrumentation, Measurement and Application (ICSIMA)*, 2017.

[93] Y. Yang, Z. Zeng, J. Cheng, and C. Guo, "An Enhanced DCO-OFDM Scheme for Dimming Control in Visible Light Communication Systems," *IEEE Photonics Journal*, vol. 8, no. 3, pp. 1–13, 2016.

[94] R. C. Kizilirmak and Y. H. Kho, "On the brightness control of ACO-OFDM based VLC systems," in *International Conference on Sensing Technology*, 2016.

[95] E. G. Rowse, S. Harris, and G. Jones, "Effects of dimming light-emitting diode street lights on light-opportunistic and light-averse bats in suburban habitats," *Royal Society open science*, vol. 5, no. 6, p. 180205, 2018.

[96] Z. Wang, W.-D. Zhong, C. Yu, J. Chen, C. P. S. Francois, and W. Chen, "Performance of dimming control scheme in visible light communication system," *Optics express*, vol. 20, no. 17, pp. 18 861–18 868, 2012.

[97] Z. Feng, C. Guo, and Y. Yang, "A Novel Hybrid Dimming Scheme for MU-MIMO-OFDM VLC System," in *ICC 2019 - 2019 IEEE International Conference on Communications (ICC)*, May 2019, pp. 1–6.

[98] Y. Yang, Z. Zeng, J. Cheng, and C. Guo, "An Enhanced DCO-OFDM Scheme for Dimming Control in Visible Light Communication Systems," *IEEE Photonics Journal*, vol. 8, no. 3, pp. 1–13, 2016.

[99] L. Wu, Z. Zhang, J. Dang, and H. Liu, "Adaptive Modulation Schemes for Visible Light Communications," *Journal of Lightwave Technology*, vol. 33, no. 1, pp. 117–125, Jan 2015.

[100] F. R. Gfeller and B. UH, "Wireless in-house data communication via diffuse infrared radiation," *Information Systems*, vol. 5, no. 11, pp. 1474–1486, 1980.

[101] J. Armstrong, "Peak-to-average power reduction for OFDM by repeated clipping and frequency domain filtering," *Electronics letters*, vol. 38, no. 5, pp. 246–247, 2002.

[102] R. Mesleh, H. Elgala, and H. Haas, "On the performance of different OFDM based optical wireless communication systems," *IEEE/OSA Journal of Optical Communications and Networking*, vol. 3, no. 8, pp. 620–628, 2011.

[103] J. Li, X.-D. Zhang, Q. Gao, Y. Luo, and D. Gu, "Exact BEP analysis for coherent M-ary PAM and QAM over AWGN and Rayleigh fading channels," in *VTC Spring 2008-IEEE Vehicular Technology Conference*. IEEE, 2008, pp. 390–394.

[104] J. Armstrong and B. J. C. Schmidt, "Comparison of Asymmetrically Clipped Optical OFDM and DC-Biased Optical OFDM in AWGN," *IEEE Communications Letters*, vol. 12, no. 5, pp. 343–345, 2008.

[105] H. Dong, H. Zhang, K. Lang, B. Yu, and M. Yao, "OFDM visible light communication transmitter based on LED array," *Chinese Optics Letters*, vol. 12, no. 5, p. 052301, 2014.

[106] J. Armstrong, "Optical domain digital-to-analog converter for visible light communications using LED arrays," *Photonics Research*, vol. 1, no. 2, pp. 92–95, 2013.

[107] M. Grant and S. Boyd, "CVX: Matlab software for disciplined convex programming, version 2.1."

[108] ——, "Graph implementations for nonsmooth convex programs," in *Recent Advances in Learning and Control*, ser. Lecture Notes in Control and Information Sciences, V. Blondel, S. Boyd, and H. Kimura, Eds. Springer-Verlag Limited, 2008, pp. 95–110, http://stanford.edu/~boyd/graph_dcp.html.

[109] ——, "CVX: Matlab software for disciplined convex programming, version 2.1," 2014.

[110] W. Yu, W. Rhee, S. Boyd, and J. M. Cioffi, "Iterative water-filling for gaussian vector multiple-access channels," *IEEE Transactions on Information Theory*, vol. 50, no. 1, pp. 145–152, 2004.

[111] J. Grubor, V. Jungnickel, and K.-D. Langer, "Adaptive optical wireless OFDM system with controlled asymmetric clipping," in *2007 Conference Record of the Forty-First Asilomar Conference on Signals, Systems and Computers*. IEEE, 2007, pp. 1896–1902.

[112] F. Yang, Y. Sun, and J. Gao, "Adaptive LACO-OFDM with variable layer for visible light communication," *IEEE Photonics Journal*, vol. 9, no. 6, pp. 1–8, 2017.